nature portfolio

Peer Review File

Copper-Catalyzed Carbon Monoxide Electrolysis under Dynamic Operation

Corresponding Author: Professor Feng Jiao

Version 0:

Reviewer comments:

Reviewer #1

(Remarks to the Author)
This manuscript provides useful insights by investigating CO electrolysis under dynamic cycling conditions, and identifies that degradation originates from carbonate accumulation and Cu oxidation. While these degradation pathways are well known in CO2/CO reduction, situating them specifically within on/off operation is valuable. The proposed 'controlled shutdown' protocol is a practical mitigation strategy, though conceptually related to previously reported 'pulse' electrolysis and current/potential modulation approaches. To strengthen the impact, the authors should explicitly benchmark their approach against prior pulse or current-control studies and discuss its broader applicability beyond Cu-based systems.
• The authors attribute performance degradation to surface reconstruction of Cu after reduction and altered surface features. However, the ECSA appears to increase after reduction, which would normally suggest enhanced rather than diminished catalytic activity. To confirm the proposed mechanism, additional post-mortem characterization, such as TEM/ED or operando surface-sensitive techniques, would strengthen the claim, and DFT analysis could clarify whether specific facet reconstructions account for the performance changes.
• The study highlights degradation mechanisms (carbonate accumulation and Cu oxidation) that indeed impair CO electrolysis under dynamic cycling. However, carbonate poisoning and Cu oxidation are not new phenomena in the CO2/CO reduction field. The CO/Cu system is known to suffer from carbonate accumulation, Cu surface oxidation, and structural changes under dynamic or high-current operation.
• How reversible is the carbonate accumulation process under CO-rich Conditions? Can the authors quantify carbonate coverage?
• The proposed controlled shutdown strategy (under slightly negative potential to avoid site blocking or oxidation) is practical and useful. However, this concept is conceptually related to pulse electrolysis and other current/potential control approaches already reported to improve catalyst stability and selectivity. The manuscript would benefit from a comprehensive comparison to these existing methods to clarify what is truly new about this strategy.
• Is 325 hours of dynamic cycling sufficient to demonstrate long-term stability for industrial relevance, or would longer testing be needed? A performance comparison table with other stabilization approaches (e.g., surface coatings, electrolyte additives, or tandem designs) would be desirable.
• How reproducible are the results across different Cu morphologies? The author only uses nanoparticles as a modeling morphology; how about foils, nanosheets, or directly using oxide-derived Cu?
• The work introduced an operational solution and correlated with TEA benefits. However, could the controlled shutdown method be applied to other CO reduction catalysts, such as Ag, Au, or Cu alloy?

Reviewer #2

(Remarks to the Author)

Reviewer #3

(Remarks to the Author)
The manuscript discusses the dynamic operation of electrochemical CO conversion to C2+ chemicals. It combines experimental investigations with molecular simulation and technoeconomic analysis to argue that dynamic operation is possible without significant catalyst degradation by applying a power-down strategy that holds the potential at values below the open circuit potential, thus inhibiting carbonate and oxide formation.

There is much merit in investigating the dynamic operation potential of electrochemical processes, especially because the premise often is they can operate economically feasibly when using renewable power (while infeasibly when using high C

grid power) and/or switch off when spot market prices are high. We know from experience this is easier said than done, and developing suitable dynamic operating strategies for electrochemical devices is thus imperative.

I believe the main contribution of this manuscript is in the experimental evaluation, which to my mind is sound, but by itself will not justify publication in Nature Catalysis. I cannot comment on the DFT (I don't have the expertise) but the TEA appears very crude and does not compare to the quality of TEAs I've previously endorsed for publication in Nature titles.

If the authors are willing to make a significant effort to improve the TEA, I'd be happy to reconsider the manuscript. Here's some guidance:

The key weakness is the sparse selection of cases - rendering the insights very specific while not allowing to draw generalisable insights - and the sheer lack of methodological information (both in the methods and in the SI).

To point 1: I understand why grid prices in Southern Australia are included - and cross referenced with Norway - but the authors will agree the selection of locations is minimal. To allow generalisability, I'd include at least 10 locations across the globe that span the envelope of possible renewable energy performance. Also, I'd look at including all 4 seasons (for countries where there are 4, otherwise select as appropriate) to include the fluctuations in renewable energy production throughout a year, plus, please don't use the values from 1 day, but take an average electricity price profile over a month (or even better evaluate the performance for each day in the month selected). Try to synthesise learning from this analysis, including on what this could mean for the number of starts/stops in a day/week/month/year, and how this reflects on the cathode performance observed.

To point 2: I expect a full explanation of the TEA method, including every little detail and every assumption on technical and economic inputs. Referring to a published paper simply won't do. Critically, it isn't clear what is included in the capex, does it include equipment costs, or installed costs, or full total capital requirement (ref the DOE/NETL cost estimation guidelines, QGESS). The reason for asking is if not all capital items were included, the capex may easily be double if not triple of what you have calculated, which may alter your analysis and optimal capacity factors quite dramatically. Idem, how was the capex discounted, was a CRF used, or were full NPV calculations done? What is a nominal interest rate? Is it the weighted average cost of capital meant? If so, please use a more realistic value between 7 and 12% (3.7% is a value a government may use, but certainly not a commercial company meaning to make a profit).

Version 1:

Reviewer comments:

Reviewer #1

(Remarks to the Author)
The authors have done a fantastic job in addressing the reviewers questions. The work is ready for publication.

Reviewer #2

(Remarks to the Author)
I have carefully reviewed the authors' responses and the revised manuscript. The authors have addressed all of my concerns and questions in a satisfactory manner. The revisions have significantly improved the clarity and quality of the work. I have no further comments and recommend the paper for publication. Figure 2 is currently not very aesthetically pleasing and could be better formatted.

Reviewer #3

(Remarks to the Author)
The reviewer appreciates the changes made to the TEA section, but it remains unclear if all relevant costs are included in the model. The question to what extent cyclic operation is economical is a critical one, and deserves careful consideration. Only if all relevant capital and operational costs are included, the analysis is meaningful. In the current rebuttal and revised manuscript, it remains unclear if they are. Authors suggest they include costs for the electrolyser, balance of plant, distillation and PSA. This is not disputed. What is unclear is if ALL costs are included for these unit operations. Referring to the DOE/NETL studies and guidelines (QGESS, I referred to this in my previous reply but the authors failed to comments on this), a full capital cost should amount at Total Capital Required, also called Total As Spent Cost. This includes equipment, installation, EPC, appropriate contingencies (not the obligatory 10% everybody adds), owner's and start up costs, and interest during construction. Only if all these capital elements are included, can a meaningful analysis of part-load operation be undertaken. From the current reply, and digging into the SI references cites (60-63 mainly), here, only the equipment and installation costs are included. If true, the real capital required would be 2-3 times higher, rendering a completely different part-load analysis.

Failing to comment on this suggests authors may be unaware of this point, which leads the reviewer to dismiss the manuscript as suitable for publication (and I even wonder if all previous Nature Catalysis and Sustainability publications using the same TEA model should not be retracted too).

I'm afraid I have to recommend against publication.

Version 2:

Reviewer comments:

Reviewer #3

(Remarks to the Author)
The authors have made a laudable and meaningful improvement to the TEA. The reviewer now also supports publication.

I'm particularly happy that even with full costs included the part-load case remains positive for Australia, and for a number of other country/season combinations (fig 5c). That's one of the first confirmations I have seen that show that operating electrochemical hydrocarbon production systems in a part-load fashion indeed makes economic sense. Well done.

Point-by-Point Response

Reviewer: 1

General Comments R1: *This manuscript provides useful insights by investigating CO electrolysis under dynamic cycling conditions, and identifies that degradation originates from carbonate accumulation and Cu oxidation. While these degradation pathways are well known in CO_2/CO reduction, situating them specifically within on/off operation is valuable. The proposed 'controlled shutdown' protocol is a practical mitigation strategy, though conceptually related to previously reported 'pulse' electrolysis and current/potential modulation approaches. To strengthen the impact, the authors should explicitly benchmark their approach against prior pulse or current-control studies and discuss its broader applicability beyond Cu-based systems.*

Response: We thank the reviewer for recognizing the importance of our study in elucidating degradation pathways during dynamic CO electrolysis and the practical significance of the proposed controlled-shutdown strategy.

We appreciate the reviewer's insightful comment regarding benchmarking our "controlled shutdown" protocol against previously reported dynamic or pulse electrolysis strategies. We have now included a detailed comparison (Supplementary Table 1) summarizing representative Cu-based dynamic operation studies in the past decade (e.g., *Timoshenko et al., Nat. Catal., 2022*; *Herzog et al., Nat. Commun., 2024*; *Kok et al., J. Am. Chem. Soc., 2024*; *Ye et al., Nat. Commun., 2024*; *Casebolt DiDomenico et al., ACS Catal., 2023*). These studies typically employ **high-frequency pulse or square-wave control** under continuous electrolysis to refresh surface Cu oxidation states or mitigate flooding. In contrast, our "controlled powerdown" method addresses a distinct challenge—**long-term intermittent power-down periods (hours–days)** arising in real renewable-driven operation, where undesired Cu oxidation and carbonate accumulation occur during idle states. This benchmarking analysis has been added to the revised SI (Page S59) and discussed in the main text (page 9), clearly delineating our contribution relative to pulse and modulation approaches.

We further expanded the discussion to highlight that the principle of maintaining a mildly reductive potential to prevent degradation can be generalized to other CO-reduction catalysts, including micro-size Cu, oxide-derived Cu, and CuAg systems. This is supported by our additional control experiment using micron-sized Cu, oxide-derived Cu, and CuAg (Supplementary Fig. 32) showing consistent stabilization behavior with potential-holding protection. We have included these explanations in the revised manuscript (page 9 and S34).

Page 9:

It is important to note that the power-down protocol proposed here is conceptually distinct from previously reported pulse or potential-modulation strategies. While prior studies[36-42] used short periodic pulses during continuous electrolysis to enhance catalytic activity, our method focuses on mitigating degradation during extended off-state periods (Supplementary Table 1). By maintaining a mild cathodic bias only when the system is powered down, the Cu catalyst is effectively protected from oxidation and carbonate accumulation, enabling reliable restart and seamless integration with intermittently available solar power. Although carbonate poisoning and Cu oxidation have been previously recognized in CO_2/CO electroreduction, this study uniquely elucidates how these degradation pathways evolve under power-down conditions and provides an effective, generalizable mitigation strategy for dynamic electrolysis.

Besides, the effect of the Cu structure was also excluded by using micro-size Cu, CuO, and CuAg alloy (Supplementary Fig. 32).

Page S59:

Supplementary Table 1 | Comparison between pulse-controlled electrolysis and the power-down strategy for Cu-based catalysts.

Ref.	Reactor, Electrolyte & Gas	Catalyst	Dynamic Control (Pulse)	Degradation / Mitigation
Blaž Tomc et al. 2025 (ChemRxiv preprint)[12]	H-cell (0.1 M $KHCO_3$, CO_2 bubbled)	Cu foil (bulk Cu)	Square-wave (–1.0 V + 2 s anodic pulses / 2 min)	Pulses cyclically oxidize/reduce Cu, keeping surface active.
Liviu C. Tănase et al. 2025 (Nat. Catal.)[13]	Custom quasi-in-situ cell (0.1 M CO_2-sat. $KHCO_3$)	Cu(100) single crystal	1 s –1.0 V / +0.6–0.8 V alternating pulses	Short anodic pulses form Cu(I)–O species, suppressing bulk oxidation.
Antonia Herzog et al. 2024 (Nat. Commun.)[14]	H-cell (0.1 M CO_2-sat. $KHCO_3$)	Pre-reduced Cu_2O nanocubes (~30 nm)	Square-wave –1.0 V / +0.6 V (0.5–15 s)	Co-adsorbed OH raises pH, stabilizing Cu_2O; optimized pulses boost C_2.
Janis Timoshenko et al. 2022 (Nat. Catal.)[15]	H-cell (0.1 M $KHCO_3$, AEM-separated)	Cu_2O nanocubes (~30 nm)	Pulses –1.0 V / +0.6 V (0.5–10 s)	Mixed Cu^0/Cu^+ interface refreshed by short anodic steps, reducing H_2.
Takashi Ito et al. 2024 (EES Catal.)[16]	Flow cell (GDE, 1 M KOH (catholyte)	Cu nanoparticle / CuO nanowire	Anodic/cathodic (E_a/Ec) or dual-cathodic pulses	Redox cycling of CuO NWs forms GBs, sustaining C_2^+ activity.
Rileigh Casebolt DiDomenico et al. 2023 (ACS Catal.)[17]	H-cell (0.1 M $KHCO_3$)	Polycrystalline Cu	–0.9 V vs 0 V square pulses (varied freq.)	CO/H balance control reduces H-poisoning; mild oxidation refreshes Cu.
Jesse Kok et al. 2024 (J. Am. Chem. Soc.)[18]	zero-gap MEA (0.5–1 M $KHCO_3$, humidified CO_2)	Sputtered Cu	–200 mA cm^{-2} w/ OCP or O_2 pulses	Oxidative pulses re-oxidize Cu, suppressing Cu migration and C–oxide buildup.
Ke Ye et al. 2024 (Nat. Commun.)[19]	H-cell (0.1 M $KHCO_3$, CO_2-sat)	Polycrystalline Cu foil	–1.1 V / +0.6 V (10 s cycles)	Pulses generate Cu^0/Cu_2O mix, enhancing C–C coupling and C_2 formation.
Our work	Zero-gap cell (1 M KOH, CO)	Cu nanoparticle	1.8~1.9 V (cell voltage, 0-3days) / 200mA/cm^2	Avoids Cu oxidation and carbonate accumulation, enabling seamless coupling with intermittently available solar energy

Page S34:

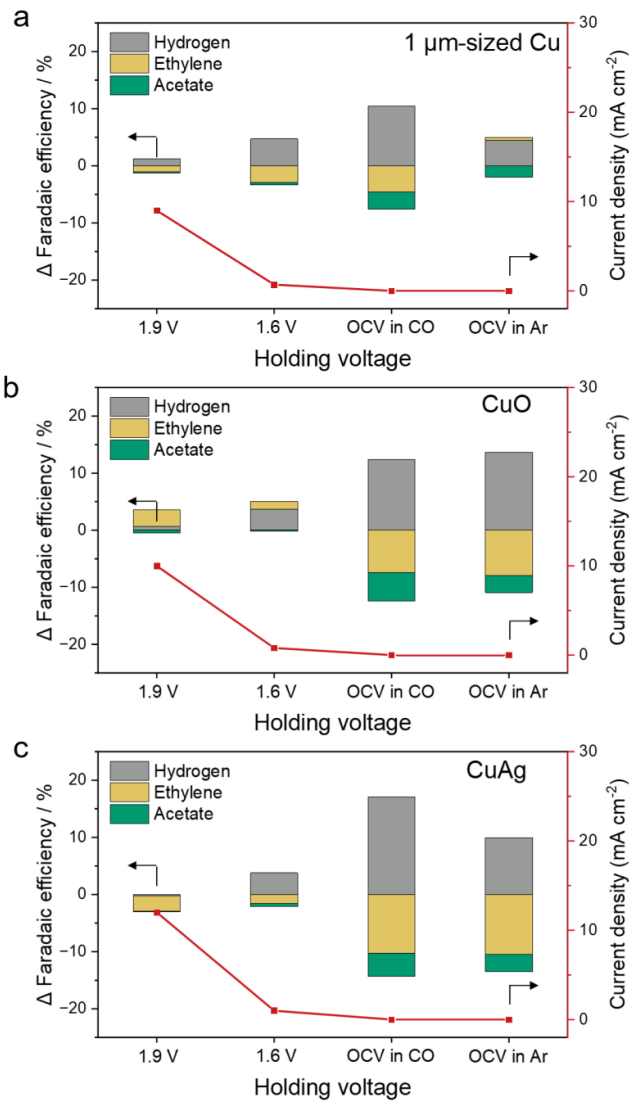

Supplementary Fig. 32 | Evaluation of the applicability of the dynamic operation strategy on other Cu based catalyst including micron-sized sized Cu, CuO, and CuAg. The same cathode preparation method was used (Copper powder, –625 mesh, APS 0.50–1.5 micron, 99%, Thermo Scientific Chemicals; Copper(II) oxide, nanopowder <50 nm, Sigma-Aldrich; Silver-copper alloy, nanopowder <100 nm particle, Sigma-Aldrich). The left y-axis shows ΔFE, and the right y-axis shows the current density at the specific holding voltage.

Specific Comment R1-1: *The authors attribute performance degradation to surface reconstruction of Cu after reduction and altered surface features. However, the ECSA appears to increase after reduction, which would normally suggest enhanced rather than diminished catalytic activity. To confirm the proposed mechanism, additional post-mortem characterization, such as TEM/ED or operando surface-sensitive techniques, would strengthen the claim, and DFT analysis could clarify whether specific facet reconstructions account for the performance changes.*

Response: We appreciate the reviewer's insightful comment. We would like to clarify that our manuscript does not attribute the observed performance degradation to Cu surface reconstruction after reduction. Under Ar atmosphere, Cu is oxidized at OCP, leading to varied activity trends after re-reduction—sometimes increasing, sometimes decreasing, or remaining nearly constant (Supplementary Fig. 13)—depending on the extent and reversibility of the oxidation–reduction process. These behaviours reflect distinct surface restructuring tendencies under continuous versus intermittent operation (Supplementary Fig. 26).

We also would like to point out that the observed increase in ECSA primarily reflects surface roughening rather than enhanced intrinsic activity or selectivity; therefore, the higher ECSA after dynamic operation under Ar does not necessarily indicate improved CO electroreduction performance.

We fully agree that post-mortem or operando characterization could further deepen the mechanistic understanding. We conducted four sets of additional TEM measurements on samples after electrochemical reduction. However, due to the catalyst layer composition (10 wt% Nafion and 10 wt% PTFE binder sprayed on carbon paper for zero-gap cell testing), reliable TEM specimen preparation was challenging—the carbon support and residual particulates interfere with imaging and diffraction quality (**Figure R1)**. Sample preparation also presents a significant challenge. Here, the catalyst was scraped from the carbon paper, followed by ultrasonic dispersion in ethanol and drop-casting onto TEM grids (**Figure R2**). This procedure can induce substantial particle fragmentation and structural perturbations, thereby obscuring or artificially altering subtle surface reconstructions and making them difficult to identify reliably.

To preserve the true surface morphology after reaction, we have included in the manuscript the SEM images of the samples collected immediately after reaction (Supplementary Fig. 8). These SEM results, together with the observed increase in ECSA, suggest that the reconstructed Cu surface does not return its original state after each cycle, leading to inconsistent performance.

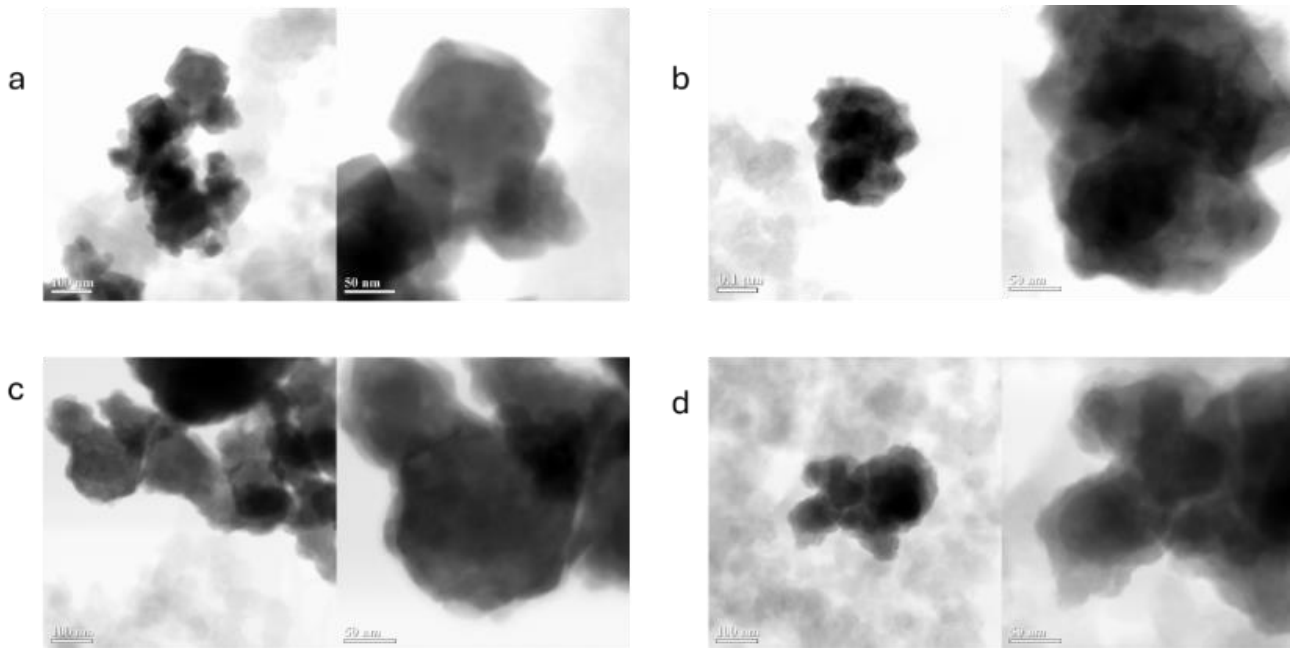

Figure R1 | TEM images of the cathode after reaction under different operating conditions. a, 200 mA cm^{-2} for 3 h. b, 200 mA cm^{-2} for 1 h, followed by 1 h power-down at 1.9 V in CO, then 200 mA cm^{-2} for 1 h. c, 200 mA cm^{-2} for 1 h, followed by 1 h at OCV in CO, then 200 mA cm^{-2} for 1 h. d, 200 mA cm^{-2} for 1 h, followed by 1 h at OCV in Ar, then 200 mA cm^{-2} for 1 h.

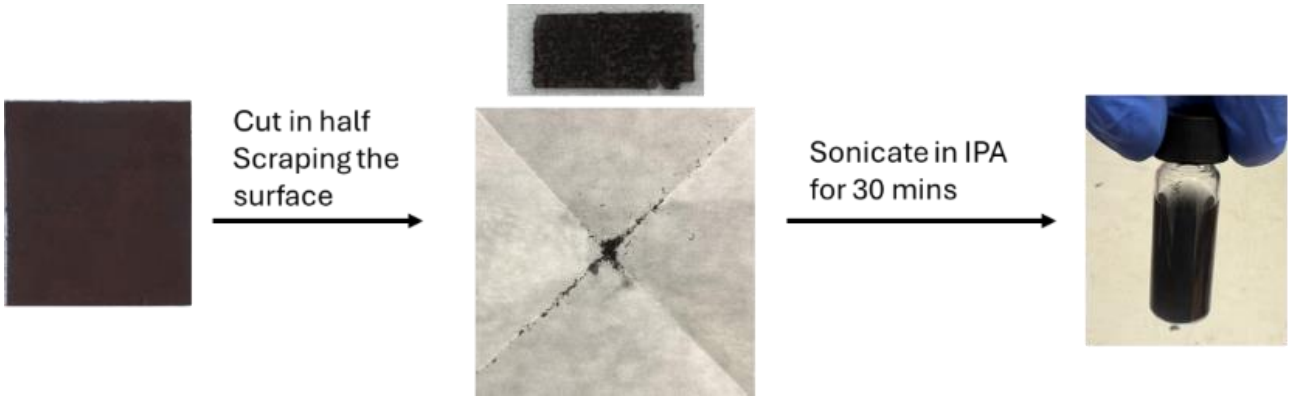

Figure R2 | Schematic illustration of the TEM sample preparation process.

Specific Comment R1-2: *The study highlights degradation mechanisms (carbonate accumulation and Cu oxidation) that indeed impair CO electrolysis under dynamic cycling. However, carbonate poisoning and Cu oxidation are not new phenomena in the CO2/CO reduction field. The CO/Cu system is known to suffer from carbonate accumulation, Cu surface oxidation, and structural changes under dynamic or high-current operation.*

Response: We appreciate the reviewer's thoughtful comment. We agree that carbonate accumulation and Cu oxidation have been previously recognized in CO_2/CO electroreduction systems. However, our work focuses on a distinct operational context—the degradation processes that occur specifically during power-down and restart cycles, which have not been systematically investigated before.

While earlier studies examined these phenomena under continuous electrolysis or short pulse modulation, our results demonstrate that carbonate accumulation and Cu oxidation proceed through different pathways during off-state conditions, leading to severe performance loss upon restart. By decoupling the effects of gas environment (CO vs Ar) and cell potential during shutdown, we were able to quantitatively correlate each degradation mechanism with its operational trigger, thereby clarifying how these known phenomena evolve under intermittent operation.

Importantly, we further propose a controlled-power down protocol, in which a mild cathodic bias effectively suppresses both carbonate precipitation and Cu oxidation, enabling full recovery after long idle periods. This strategy thus transforms well-known degradation processes into controllable and reversible phenomena, advancing practical dynamic CO electrolysis under renewable operation scenarios. We appreciate the reviewer for pointing this out, and we have added further clarification in the revised manuscript (Page 9).

Page 9:

It is important to note that the power-down protocol proposed here is conceptually distinct from previously reported pulse or potential-modulation strategies. While prior studies[36-42] used short periodic pulses during continuous electrolysis to enhance catalytic activity, our method focuses on mitigating degradation during extended off-state periods (Supplementary Table 1). By maintaining a mild cathodic bias only when the system is powered down, the Cu catalyst is effectively protected from oxidation and carbonate accumulation, enabling reliable restart and seamless integration with intermittently available solar power. Although carbonate poisoning and Cu oxidation have been previously recognized in CO_2/CO electroreduction, this study uniquely elucidates how these degradation pathways evolve under power-down conditions and provides an effective, generalizable mitigation strategy for dynamic electrolysis.

Specific Comment R1-3: *How reversible is the carbonate accumulation process under CO-rich Conditions? Can the authors quantify carbonate coverage?*

Response: We thank the reviewer for these important questions. Under CO-rich conditions, the carbonate accumulation process on Cu is not fully reversible. As shown in Supplementary Fig. 10, when the electrolyzer was held at OCP in CO for 10 minutes (repeated three times), the catalyst required more than 20 hours to recover its initial activity after the first two OCP periods, and became completely deactivated after the third. These results clearly indicate that the carbonate species adsorbed on Cu cannot be fully removed upon re-applying bias, and their progressive accumulation leads to irreversible surface passivation during dynamic operation. We have added this explanation in the manuscript (Page S11 and S67)

Direct quantification of carbonate coverage is experimentally challenging because the carbonate layer forms at the buried catalyst–electrolyte interface in the gas diffusion layer of the zero-gap cell. Although in-situ Raman spectroscopy confirmed the formation of carbonate species on Cu under OCP conditions, quantitative evaluation of carbonate coverage remains challenging. During electrolysis at 200 mA cm^{-2}, strong gas bubble evolution interferes with Raman signal collection, and after high-current operation, the bubbles and surface roughness also make it difficult to obtain stable spectra under subsequent OCP conditions. Therefore, due to these experimental limitations, it is not feasible to accurately quantify carbonate coverage in the current setup.

Page S11:

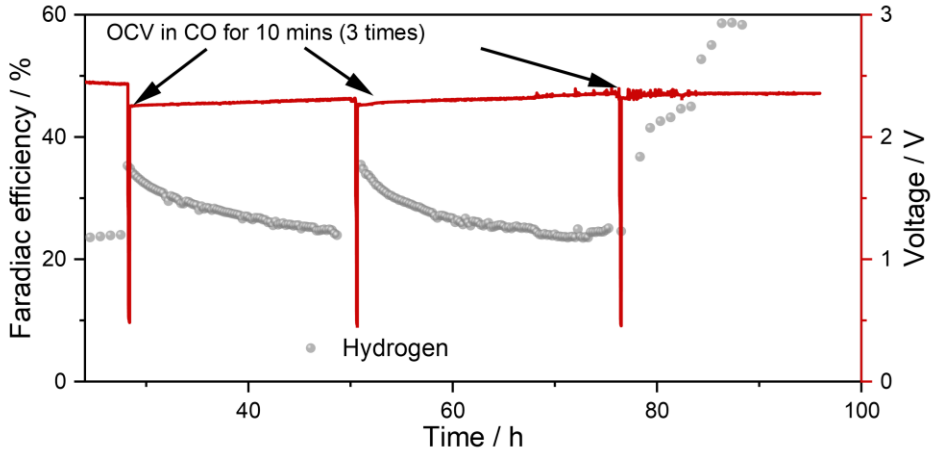

Supplementary Fig. 10 | Activity decay upon repeated OCP interruptions under CO atmosphere. Three consecutive 10-minute OCP periods cause progressive loss of Faradaic efficiency, confirming partial irreversibility of carbonate accumulation.

Page S67:

Notably, the carbonate accumulation process on Cu is only partially reversible—while some carbonate species can be removed at 200 mA cm^{-2}, prolonged exposure under CO-rich OCP conditions leads to irreversible surface passivation and incomplete activity recovery (Supplementary Fig. 10).

Specific Comment R1-4: *The proposed controlled shutdown strategy (under slightly negative potential to avoid site blocking or oxidation) is practical and useful. However, this concept is conceptually related to pulse electrolysis and other current/potential control approaches already reported to improve catalyst stability and selectivity. The manuscript would benefit from a comprehensive comparison to these existing methods to clarify what is truly new about this strategy.*

Response: We thank the reviewer for recognizing the usefulness of our study in elucidating degradation pathways during dynamic CO electrolysis and for highlighting the practical significance of the proposed controlled-shutdown strategy.

We appreciate the reviewer's insightful comment regarding benchmarking our "controlled-shutdown" protocol against previously reported dynamic or pulse-electrolysis approaches. In response, we have now included a detailed comparison (Supplementary Table 1) summarizing representative Cu-based dynamic-operation studies in the past decade (e.g., *Timoshenko et al., Nat. Catal.* 2022; *Herzog et al., Nat. Commun.* 2024; *Kok et al., J. Am. Chem. Soc.* 2024; *Ye et al., Nat. Commun.* 2024; *Casebolt-DiDomenico et al., ACS Catal.* 2023). These studies typically employ short, high-frequency pulse or square-wave control during continuous electrolysis to refresh Cu oxidation states or tune product selectivity.

In contrast, our controlled-power down method addresses a fundamentally different challenge—long-term, intermittent power-down periods (hours to days) that occur in renewable-driven operation, where Cu oxidation and carbonate accumulation take place during idle states. By maintaining a mild cathodic bias only when the system is powered down, our protocol effectively prevents both degradation pathways and ensures full performance recovery upon restart.

This benchmarking analysis has been added to the revised SI (Supplementary Table 1) and discussed in the main text (page 9), clearly delineating our contribution relative to previously reported pulse- and modulation-based strategies.

Page 9:

It is important to note that the power-down protocol proposed here is conceptually distinct from previously reported pulse or potential-modulation strategies. While prior studies[36-42] used short periodic pulses during continuous electrolysis to enhance catalytic activity, our method focuses on mitigating degradation during extended off-state periods (Supplementary Table 1). By maintaining a mild cathodic bias only when the system is powered down, the Cu catalyst is effectively protected from oxidation and carbonate accumulation, enabling reliable restart and seamless integration with intermittently available solar power. Although carbonate poisoning and Cu oxidation have been previously recognized in CO_2/CO electroreduction, this study uniquely elucidates how these degradation pathways evolve under power-down conditions and provides an effective, generalizable mitigation strategy for dynamic electrolysis.

Page S58:

Supplementary Table 1 | Comparison between pulse-controlled electrolysis and the power-down strategy for Cu-based catalysts.

Ref.	Reactor, Electrolyte & Gas	Catalyst	Dynamic Control (Pulse)	Degradation / Mitigation
Blaž Tomc et al. 2025 (ChemRxiv preprint)[12]	H-cell (0.1 M $KHCO_3$, CO_2 bubbled)	Cu foil (bulk Cu)	Square-wave (–1.0 V + 2 s anodic pulses / 2 min)	Pulses cyclically oxidize/reduce Cu, keeping surface active.
Liviu C. Tănase et al. 2025 (Nat. Catal.)[13]	Custom quasi-in situ cell (0.1 M CO_2-sat. $KHCO_3$)	Cu(100) single crystal	1 s –1.0 V / +0.6–0.8 V alternating pulses	Short anodic pulses form Cu(I)–O species, suppressing bulk oxidation.
Antonia Herzog et al. 2024 (Nat. Commun.)[14]	H-cell (0.1 M CO_2-sat. $KHCO_3$)	Pre-reduced Cu_2O nanocubes (~30 nm)	Square-wave –1.0 V / +0.6 V (0.5–15 s)	Co-adsorbed OH raises pH, stabilizing Cu_2O; optimized pulses boost C_2.
Janis Timoshenko et al. 2022 (Nat. Catal.)[15]	H-cell (0.1 M $KHCO_3$, AEM-separated)	Cu_2O nanocubes (~30 nm)	Pulses –1.0 V / +0.6 V (0.5–10 s)	Mixed Cu^0/Cu^+ interface refreshed by short anodic steps, reducing H_2.
Takashi Ito et al. 2024 (EES Catal.)[16]	Flow cell (GDE, 1 M KOH (catholyte)	Cu nanoparticle / CuO nanowire	Anodic/cathodic (E_a/E_c) or dual-cathodic pulses	Redox cycling of CuO NWs forms GBs, sustaining C_2^+ activity.
Rileigh Casebolt DiDomenico et al. 2023 (ACS Catal.)[17]	H-cell (0.1 M $KHCO_3$)	Polycrystalline Cu	–0.9 V vs 0 V square pulses (varied freq.)	CO/H balance control reduces H-poisoning; mild oxidation refreshes Cu.
Jesse Kok et al. 2024 (J. Am. Chem. Soc.)[18]	zero-gap MEA (0.5–1 M $KHCO_3$, humidified CO_2)	Sputtered Cu	–200 mA cm^{-2} w/ OCP or O_2 pulses	Oxidative pulses re-oxidize Cu, suppressing Cu migration and C–oxide buildup.
Ke Ye et al. 2024 (Nat. Commun.)[19]	H-cell (0.1 M $KHCO_3$, CO_2-sat)	Polycrystalline Cu foil	–1.1 V / +0.6 V (10 s cycles)	Pulses generate Cu^0/Cu_2O mix, enhancing C–C coupling and C_2 formation.
Our work	Zero-gap cell (1 M KOH, CO)	Cu nanoparticle	1.8~1.9 V (cell voltage, 0-3days) / 200mA/cm^2	Avoids Cu oxidation and carbonate accumulation, enabling seamless coupling with intermittently available solar energy

Specific Comment R1-5: *Is 325 hours of dynamic cycling sufficient to demonstrate long-term stability for industrial relevance, or would longer testing be needed? A performance comparison table with other stabilization approaches (e.g., surface coatings, electrolyte additives, or tandem designs) would be desirable.*

Response: We appreciate the reviewer's constructive comment. We agree that industrially relevant CO or CO_2 electrolysis would ultimately require operation over thousands of hours. In the revision manuscript, we have retest two cells, one could achieve 750 hours and the other one could achieve 550 hours at least. This represents one of the longest reported stability tests under intermittent operation, equivalent to more than 31 days of repeated power-on/power-down cycles, and is sufficient to validate the mechanistic reversibility and mitigation effectiveness of the proposed controlled-shutdown strategy.

Continuous long-term operation under laboratory dynamic-cycling conditions is strongly constrained by experimental logistics (e.g., gas delivery stability, electrolyte carbonation, and cell sealing durability). Nonetheless, the constant Faradaic efficiency and cell voltage profiles over 750 h indicate that no measurable degradation accumulates during repeated shutdowns, implying that our mitigation concept can be extended to longer timescales.

To address the reviewer's suggestion, we have added Supplementary Table 2, which benchmarks our strategy against other reported stability, highlighting that our controlled-shutdown method achieves comparable or better stability without catalyst modification or chemical additives, thereby offering a more general and practical solution for renewable-powered CO electrolysis. We have added the relative part in the manuscript (Page 2, 3, 9, 10, S36 and S59)

Page 2:

This strategy enables stable dynamic operation for more than 750 hours without any significant performance loss.

Page 3:

This approach significantly enhances system stability, achieving minimal performance loss over 750 hours of operation with 31 repeated power cycles.

Page 9:

This method enabled stable dynamic operation over 750 hours of operation with 31 repeated power cycles, during which time FE of hydrogen remained at 20% (Fig. 4c), while FE of C_{2+} product was maintained at 75% (Supplementary Fig. 35).

Page 10:

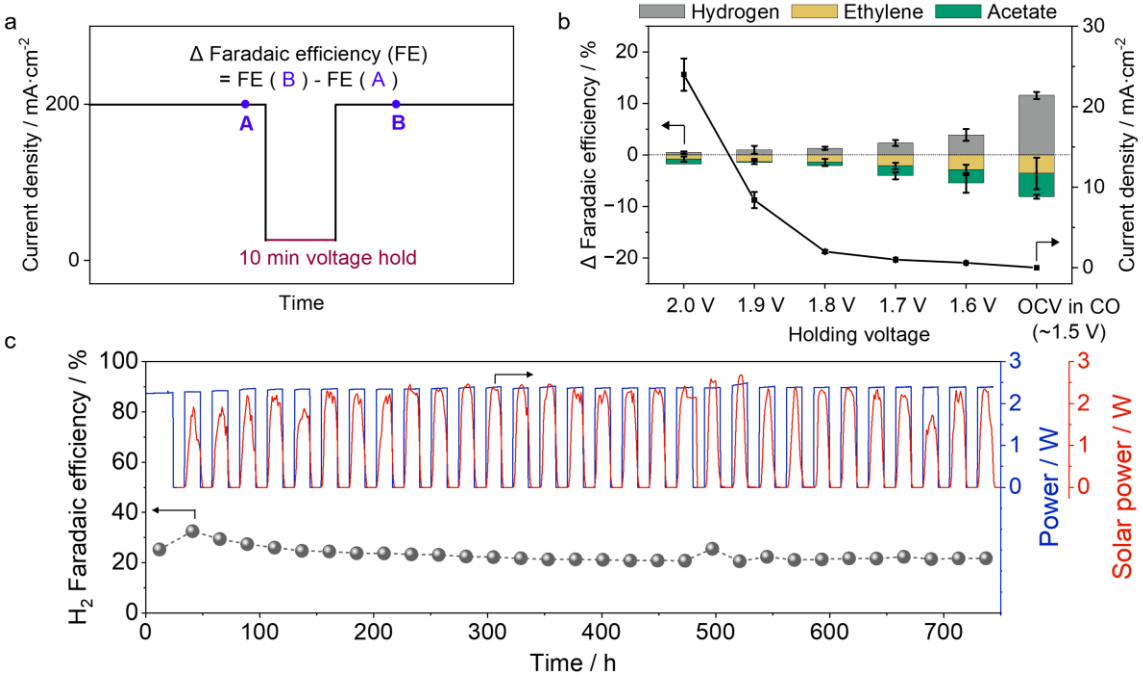

Fig. 4 | Stable dynamic operation achieved by maintaining the copper catalyst within a protective voltage during power-down periods. a | Schematic illustration of the dynamic operation method (see Methods for more details). **b** | Impact of various holding voltages on Faradaic efficiency change (ΔFE) and the corresponding current density during the power-down period. **c** | Demonstration of stable CO electrolyzer dynamic operation between 200 mA cm^{-2} and 1.9 V in CO, following the solar power trend. The solar power profile is sourced from the U.S. Energy Information Administration for July 1st to August 4th, 2024.[19] The actual power data was scaled down by a factor of 2×10^8 to match the power capacity of our reactor. Carbon product stability and voltage data are provided in Supplementary Fig. 35a.

Page S35:

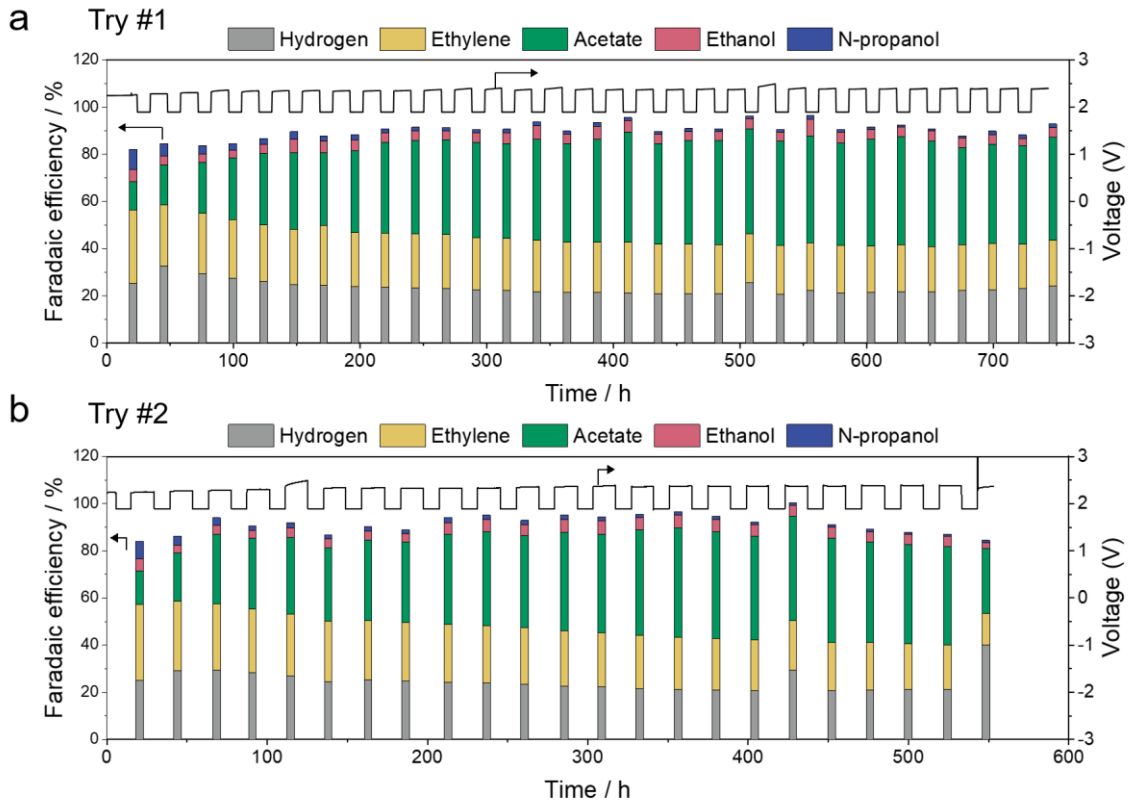

Supplementary Fig. 35 | Faradaic efficiency and voltage over time during dynamic operation between 200 mA cm^{-2} and 1.9 V in CO. Measurements were performed in a 5 cm^2 zero-gap CO electrolyzer in 1 M KOH for two times**.** The system demonstrated stable performance for 750 hours, maintaining a C_{2+} Faradaic efficiency of approximately 75% and a voltage of 2.35 V. For "Try #2" in panel **b**, the experiment was compromised due to accidental drying of the cell during anolyte replacement.

Page S59:

Supplementary Table 2. Comparison of stability performance of CO electrolysis systems

Operation mode of dynamic operation	Stability (h)	Single cell reaction area (cm^2)	Current density (mA/cm^2)	Voltage (V)	Cathode catalyst	Anolyte	Ref
No	120	5	200	2.3	Cu	3 M KOH	10.1038/s41929-022-00828-w
No	125	100	300	2.25	Cu	2 M KOH	10.1038/s44286-024-00076-8
No	18	1	100	2.5	Ag-Cu_2O	1 M NaOH	10.1038/s44160-023-00259-w
No	500	5	500	3.5	Cu-Pd	1 M KOH	10.1038/s41929-022-00757-8; Nat Catal 5, 251–258 (2022).
No	6	5	500	2.42	Cu	2 M KOH	10.1016/j.checat.2022.10.026
No	820	1	100	2.5	Cu-Ag	2.5 M KOH	10.1038/s41586-023-05918-8
No	150	2.25	400	5	silver-doped Cu_2O	H_2O	10.1038/s44160-024-00621-6
No	140	4	200	3	Cu	0.1 M CsOH	10.1038/s41929-023-01034-y
No	750	100	200	2.4	Cu 40-60nm	2M KOH	10.1038/s41467-025-63004-1
Yes	750	5	200	1.9 ~2.4	Cu 40-60nm	1 M KOH	**This Work**

Specific Comment R1-6: *How reproducible are the results across different Cu morphologies? The author only uses nanoparticles as a modelling morphology; how about foils, nanosheets, or directly using oxide-derived Cu?*

Response: We thank the reviewer for this important comment. In the revised manuscript, we have expanded our study to include oxide-derived Cu (obtained by in situ reduction of CuO) as an additional catalyst system. We observe that the proposed dynamic operation strategy remains effective for OD-Cu, demonstrating comparable stability under intermittent operation, which supports the generality of this approach across different Cu morphologies.

Cu nanoparticles and micro-size Cu were initially employed as a model catalyst system due to their compatibility with zero-gap membrane electrode assembly (MEA) architectures and their reproducible fabrication as gas diffusion electrodes (GDEs). In contrast, Cu foils are not readily applicable in zero-gap cells, as they cannot be directly implemented as GDEs. Although Cu nanosheets have been explored in prior studies, their limited commercial availability in CO electrolysis.

To ensure both practical relevance and industrial applicability, we therefore selected commercial micrometer-scale Cu and CuO as representative catalyst systems. The consistent performance observed across these catalysts indicates that the effectiveness of dynamic operation is not morphology-specific, but rather originates from the regulation of interfacial conditions during operation. We have added the further discussion in the manuscript (Page 9 and S33)

Page 9:

Cu structure was also excluded by using micro-size Cu, CuO, and CuAg alloy (Supplementary Fig. 32).

Page S33:

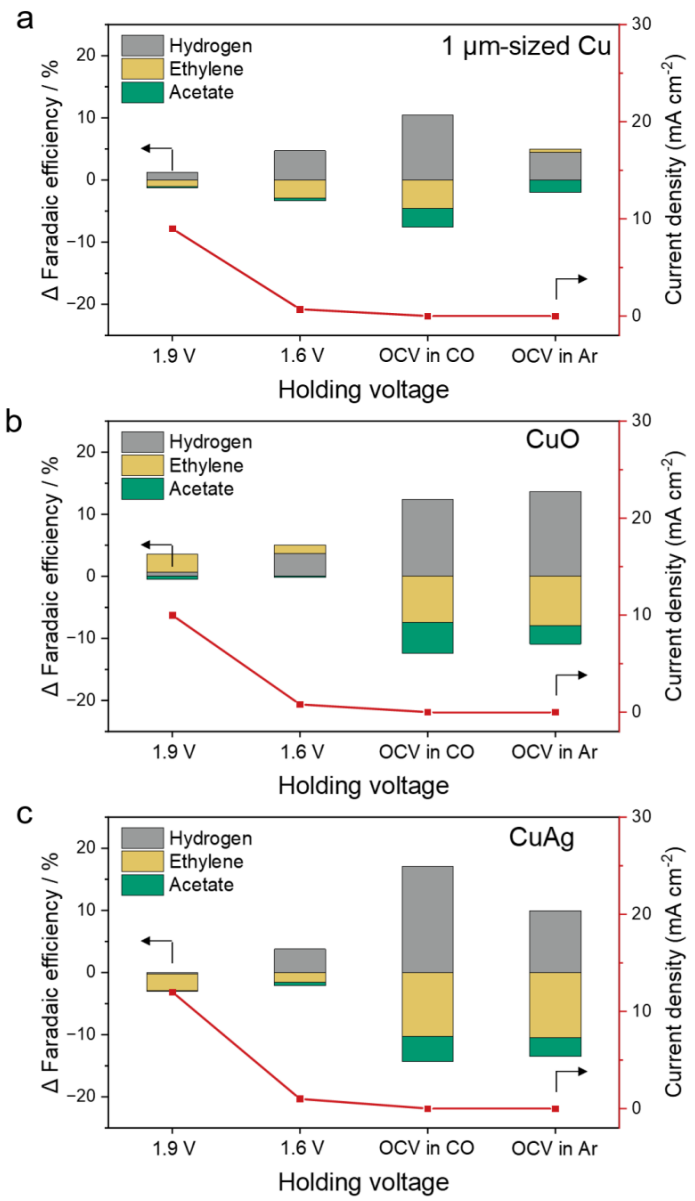

Supplementary Fig. 32 | Evaluation of the applicability of the dynamic operation strategy on other Cu based catalyst including micron-sized sized Cu, CuO, and CuAg. The same cathode preparation method was used (Copper powder, –625 mesh, APS 0.50–1.5 micron, 99%, Thermo Scientific Chemicals; Copper(II) oxide, nanopowder <50 nm, Sigma-Aldrich; Silver-copper alloy, nanopowder <100 nm particle, Sigma-Aldrich). The left y-axis shows ΔFE, and the right y-axis shows the current density at the specific holding voltage.

Specific Comment R1-7: *The work introduced an operational solution and correlated with TEA benefits. However, could the controlled shutdown method be applied to other CO reduction catalysts, such as Ag, Au, or Cu alloy?*

Response: We thank the reviewer for this insightful question. To evaluate the general applicability of the controlled shutdown strategy beyond pure Cu catalysts, we tested a commercial CuAg alloy catalyst under identical dynamic operation conditions. We find that the proposed strategy remains effective for the CuAg system, indicating that the controlled shutdown approach is not limited to a single Cu. However, this study focuses specifically on electrochemical CO reduction, where Cu-based catalysts are uniquely capable of sustaining high activity toward multicarbon products. Catalysts such as Ag and Au are primarily

selective for CO formation during CO_2 reduction rather than CO reduction, and therefore fall outside the scope of the present work. For this reason, we do not include Ag or Au catalysts in this study.

Overall, these results suggest that the controlled shutdown strategy is broadly applicable to Cu-based CO reduction catalysts, and its effectiveness arises from the regulation of operating conditions and interfacial chemistry rather than from catalyst-specific electronic effects. We have added the further discussion in the manuscript (Page 9 and S33)

Reviewer: 2

General Comments R2: *This manuscript proposes and validates that under dynamic electrolysis conditions (mimicking fluctuating renewable electricity), Cu cathodes undergo deactivation due to surface CO oxidation during shutdown, leading to the formation of (bi)carbonate, or through oxidation into Cu2O at open-circuit potential under an inert atmosphere. To address this issue, the authors introduce a mitigation strategy by maintaining a slightly negative potential relative to OCP (corresponding to ~1.8-1.9 V for the full cell) during shutdown, which effectively suppresses carbonate formation and oxidation. Experimentally, this approach enables stable dynamic operation for more than 300 hours, accompanied by a techno-economic analysis (TEA) that demonstrates its feasibility. The study integrates in-situ Raman, CV, XAS, DFT, and TEA, presenting a comprehensive investigation with practical engineering relevance. Nonetheless, a few important issues remain to be clarified.*

Response: We thank the reviewer for the positive evaluation and insightful summary.

Specific Comment R2-1: *The main experiments employ commercial Cu powder (40-60 nm), with a small amount of micron-sized Cu as a comparison. However, Cu in practice exhibits diverse surface structures, crystal facets, roughness, and oxide-derived precursors, all of which can significantly influence CO adsorption, OH* adsorption, and the propensity for carbonate formation.*

Response: We thank the reviewer for this important comment. We fully agree that Cu surface structure, crystal facets, roughness, and oxide-derived precursors can strongly influence local adsorption behavior and reaction pathways in CO reduction. To address the reviewer's concern regarding catalyst diversity, we have expanded the revised manuscript to include oxide-derived Cu (obtained by in situ reduction of CuO), commercial micrometer-scale Cu, and commercial CuAg alloy in addition to nanoscale Cu powders. Despite their distinct initial structures and surface characteristics, we observe consistent improvements in stability under controlled shutdown and dynamic operation across all tested Cu-based catalysts. This suggests that the effectiveness of the proposed strategy is robust with respect to catalyst morphology and precursor state.

Overall, while catalyst structure undoubtedly affects intrinsic activity and selectivity, our results indicate that the proposed dynamic operation and controlled shutdown strategy provides a generally applicable and complementary approach to improving device stability, independent of detailed Cu surface structure. We have added the further discussion in the manuscript (Page 9 and S33)

Page 9:

Cu structure was also excluded by using micro-size Cu, CuO, and CuAg alloy (Supplementary Fig. 32).

Page S33:

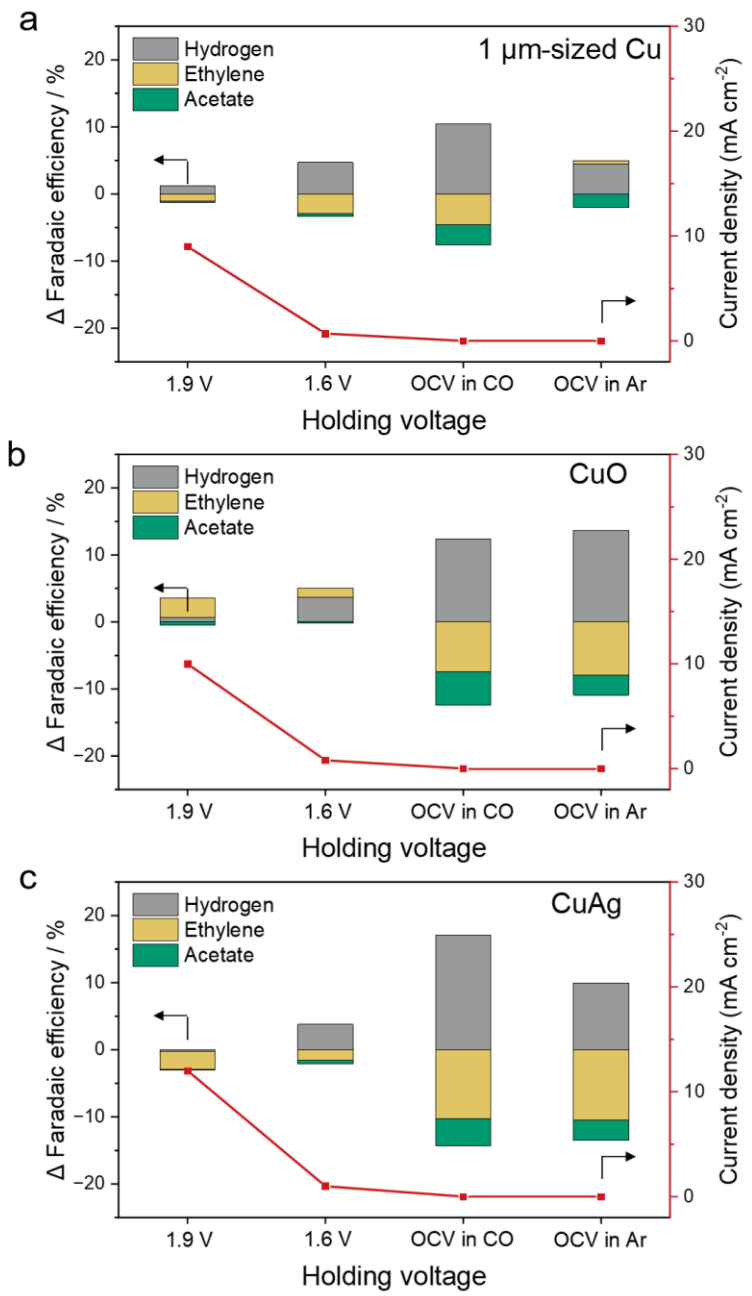

Supplementary Fig. 32 | Evaluation of the applicability of the dynamic operation strategy on other Cu based catalyst including micron-sized sized Cu, CuO, and CuAg. The same cathode preparation method was used (Copper powder, –625 mesh, APS 0.50–1.5 micron, 99%, Thermo Scientific Chemicals; Copper(II) oxide, nanopowder <50 nm, Sigma-Aldrich; Silver-copper alloy, nanopowder <100 nm particle, Sigma-Aldrich). The left y-axis shows ΔFE, and the right y-axis shows the current density at the specific holding voltage.

Specific Comment R2-2: *During power-down the authors reduce the CO feed to 2 mL·min⁻¹ and the anolyte flow to 0.1 mL·min⁻¹ while maintaining the full-cell potential at 1.9 V. It is unclear whether this 'reduced-flow + maintained-potential' protocol is practicable at industrial scale or whether the TEA fully accounts for the operational implications of such an approach.*

Response: We thank the reviewer for raising this important question regarding the practicality of the proposed operation protocol. From an industrial perspective, lowering the flow rates during the power-down period is primarily intended to reduce auxiliary energy consumption, which can be easily implemented by adjusting pump power settings. If a facility's pumps cannot modulate flow, maintaining the original flow rates would not negatively impact dynamic operation performance—thus, the flow reduction is an optional, cost-saving measure rather than a requirement.

With regard to the maintained-potential strategy, it is worth noting that in industrial PEM water electrolysis, applying a small standby bias is a well-recognized practice to protect the electrodes and maintain system performance during transient or idle operation (see Sayed-Ahmed *et al.*, *Renew. Sustain. Energy Rev.* 2024, *189*, 113883). This industrial experience confirms that maintaining a mild potential is a technically feasible and effective way to safeguard electrolyzer components during non-operating periods.

For the TEA for dynamic operation, we included the electricity required during the power-down period to maintain the potential, using the average electricity price during that period. Details of the TEA are provided in Supplementary Note 3 (pages S70-S78), and the electricity price calculations for the dynamic operation cases are specifically described on pages S74-S75.

Page S74-75:

1. Electricity cost for electrolyzer operation (100% capacity):

$$Electricity\ cost\ for\ electrolyzer\ operation\ \left(\frac{USD}{day}\right) = Power\ needed\ (MW) \times \frac{24h}{day} \times electricity\ price\ \left(\frac{USD}{kWh}\right) \quad (19)$$

where:

$$Power\ needed = Cell\ voltage\ \times\ Total\ current\ needed \quad (20)$$

Where total current needed is calculated using equation (7).

The cell voltage was 2.35 V, and the acetate selectivity was 50%, following the durability test result (Fig. 4a). For dynamic operation, the acetic acid production rate was adjusted according to the operating capacity, resulting in corresponding changes to the total current. The electricity price was also adjusted based on the operating capacity.

2. Electricity cost for power-down:

$$Electricity\ cost_{power\ down}\left(\frac{USD}{day}\right) = Power\ needed_{power\ down}\ (MW) \times Time_{power\ down}\frac{h}{day} \times Electricity\ price_{power\ down}\left(\frac{USD}{kWh}\right) \quad (21)$$

The electricity price used for power-down was the average electricity price during the power-down period, excluding the electricity price during power-on. The current density and voltage during power-down were 10 mA cm^{-2} and 1.9 V, respectively, based on our power-down experiments (Supplementary Fig. 35a). The electrolyzer area determined from the continuous operation at 50,000 kg day^{-1} (equation (6)) was used to calculate the power needed during power-down.

Power-down time was calculated as:

$$Time_{power\ down} = 24h - Time_{power\ on} \quad (22)$$

For example, at 75% capacity, the power-on time is 18 h and the power-down time is 6 h.

Specific Comment R2-3: *The SERS spectra exhibit a peak at 1085 cm⁻¹, which the authors assign to carbonate species. However, no direct evidence of transient CO_2 release during OCP or quantitative monitoring of the chemical species via online analysis is provided. The author should detect whether there is a CO_2 overflow peak in the OCP phase and verify the chemical bonding state and coverage of surface carbonate/carbonate ions or use ATR-FTIR to further confirm the carbonic acid/bicarbonate peak.*

Response: We thank the reviewer for this insightful comment. The SERS peak at 1085 cm^{-1} is assigned to *carbonate species* based on previous literature and our control experiments. Under our testing conditions (1 M KOH), any CO_2 generated from surface CO oxidation would be rapidly neutralized to CO_3^{2-} in the alkaline electrolyte, and thus no transient CO_2 release can be detected in the gas phase during OCP. This explains the absence of a CO_2 overflow peak in our on-line analysis.

To further verify the formation of carbonate species, we performed in-situ ATR-FTIR measurements. However, due to the strong reactivity of the Si-based crystal with concentrated alkaline media, ATR-FTIR experiments could not be stably conducted in 1 M KOH. We therefore repeated the measurements in 0.1 M KOH as an approximate condition. The spectra indeed showed an emerging band near 1435 cm^{-1}, which we tentatively assign to $*CO_3^{2-}$ species, accompanied by a decrease in the *CO*-related signal as the potential was increased (Figure R3a).

Nevertheless, it is important to note that the ATR-FTIR environment (0.1 M KOH with a thin Au underlayer beneath the Cu film) differs significantly from both the Raman configuration and the zero-gap MEA operating conditions (1 M KOH without an Au underlayer). These discrepancies in electrolyte concentration, local pH environment, and electrode architecture inevitably shift the absolute potentials at which surface species appear. Consequently, while the voltage-dependent evolution of the $*CO_3^{2-}$ band is qualitatively consistent across techniques, the absolute potentials should not be directly compared.

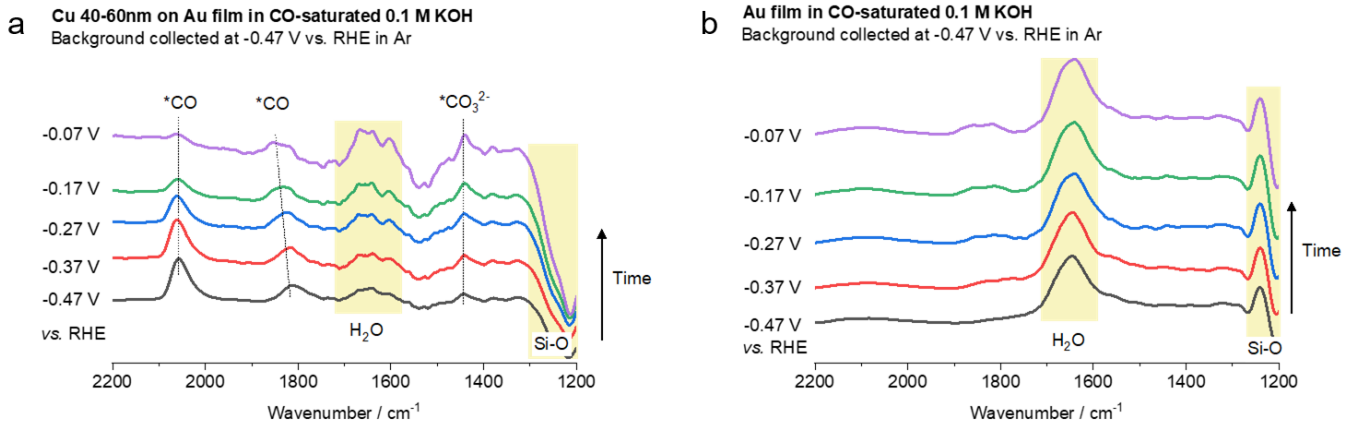

Figure R3 | *In-situ* ATR-FTIR spectra of surface species evolution under CO atmosphere. (a) Cu (40–60 nm) film deposited on Au substrate and (b) bare Au film, both recorded in 0.1 M KOH with continuous CO flow. The background spectrum was collected at –0.37 V vs. RHE in Ar. Spectra were acquired during a potential sweep from –0.37 V to –0.07 V vs. RHE each potential was stable for 3 min before collection the spectrums.

Specific Comment R2-4: *The long-term stability and durability data (>cs300 h) appear to be derived from a single demonstration, with no information provided on the number of repetitions or the associated error margins. For claims of "industrializable" stability, reproducibility data are indispensable.*

Response: We appreciate the reviewer's suggestion. Please see R1-5 for similar response.

Specific Comment R2-5: *When the power-down period is extended to 7 days, the performance becomes irreversible, indicating the presence of irreversible damage. Is this irreversible degradation still attributable to carbonate poisoning? If so, why cannot it be recovered in the same manner as short-term shutdown? If not, what are the underlying causes?*

Response: Thank you for this important question. To clarify whether a prolonged power-down period leads to irreversible degradation, we repeated the 7-day power-down experiment and closely monitored the recovery behavior after power-on. In this study, the electrolyzer was first stabilized at 200 mA cm^{-2} for 24 hours, followed by a 24-hour power-down period. After the cell performance recovered under 200 mA cm^{-2}, we initiated the full 7-day power-down cycle. This sequence was repeated twice to ensure reproducibility (Supplementary Fig. 34a).

In the newly conducted experiment, we found that after a 7-day power-down period, the H_2 Faradaic efficiency fully recovered to its original level within 10 h (with only a ~1% increase), and the C_{2+} Faradaic efficiency also returned to a comparable value (within ~3% decrease). These results indicate that a 7-day power-down does not cause permanent loss of catalytic performance; the system can indeed recover after a short period of resumed operation. To further ensure reproducibility, we subjected the same cell to a second 7-day power-down cycle. Again, after power-on, the cell fully recovered within 12 h. The consistent recovery in two independent 7-day power-down cycles demonstrates that even extended power-down periods to 7 days do not lead to irreversible degradation.

We note that the earlier 7-day power-down result that appeared irreversible was because the cell was dried out due to the pump power down, which will cause the irreversible degradation (Supplementary Fig. 54). We have added the modification in the manuscript (Page 9, S34 and S35).

Page 9:
When the power-down duration was extended to 7 days, the performance was still recoverable with longer recover time (>5 hours).

Supplementary Page 34:

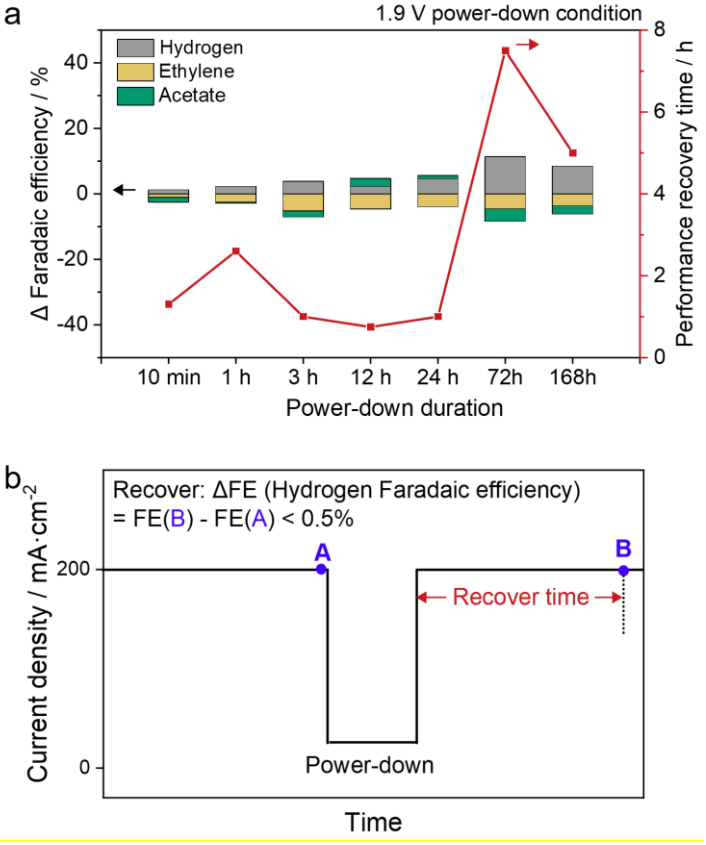

Supplementary Fig. 33 | Exploration of power-down duration in dynamic operation. a | Power-down operation at 1.9 V in CO**.** The left y-axis shows ΔFE, and the right y-axis shows the performance recovery time. **b |** Performance recovery time was defined as the duration required for the ΔFE of hydrogen (calculated as $FE_{after\ power\text{-}down} - FE_{before\ power\text{-}down}$) to fall below 0.5%.

Page S35:

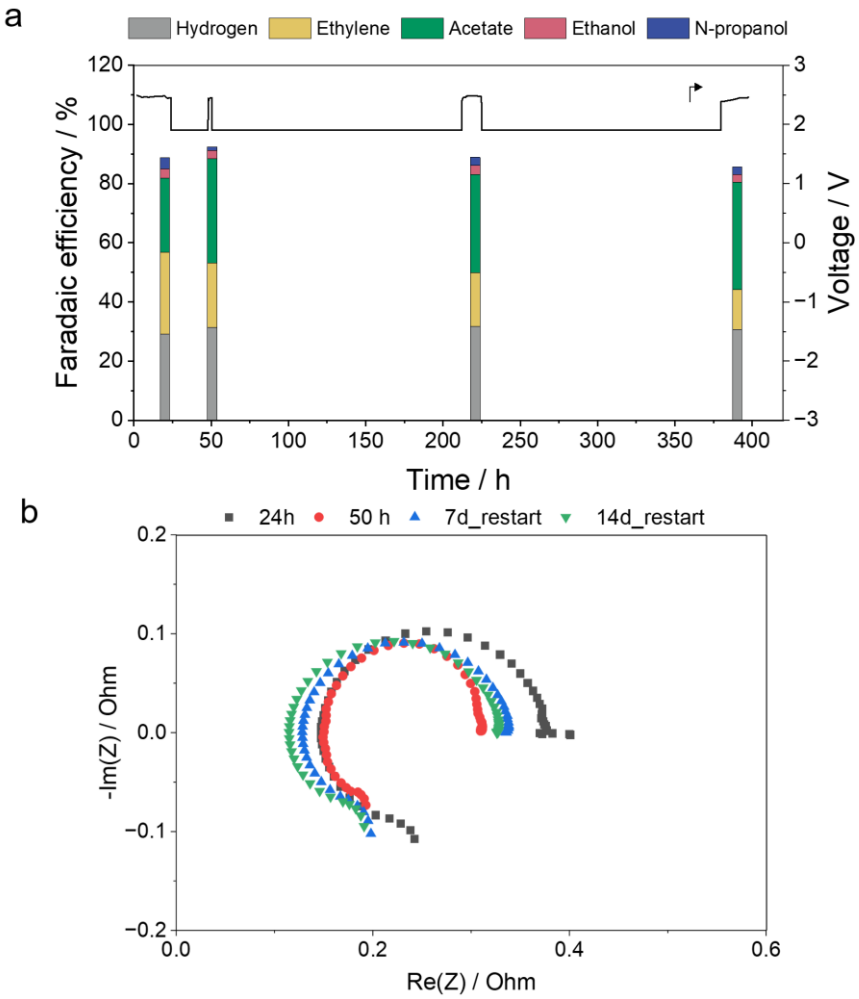

Supplementary Fig. 34 | Electrochemical impedance spectra of the CO electrolyzer at different stages of dynamic operation. a | Power-down operation at 1.9 V in CO for 7days two times**. b |** Nyquist plots collected after 24 h of initial stabilization (black), 50 h of operation (red), after the first 7-day power-down cycle (green), and after the second 7-day power-down cycle (purple) in Pannel a.

Specific Comment R2-6: *Applying a protective potential inevitably alters the overall cell state and may exert long term effects on the NiFeOx anode or the membrane. However, the manuscript does not provide long-term monitoring data on membrane impedance or anode stability.*

Response: We appreciate the reviewer's suggestion. To address this concern, electrochemical impedance spectroscopy (EIS) of full cell was conducted at different stages of the durability test to evaluate changes in overall cell resistance. The Nyquist plots remain highly similar over time. The black curve (after 24 h of initial stabilization) shows a characteristic semicircle corresponding to the charge-transfer resistance. After 50 h of operation (red), the semicircle becomes slightly smaller, indicating a modest decrease in charge-transfer resistance, which is likely attributable to the continued activation and restructuring of the Cu catalyst during early operation. After a 7-day power-down cycle (green), only a slight shift is observed, and the semicircle size remains comparable to that of the earlier datasets, suggesting minimal impact from the extended

shutdown. Even after two consecutive 7-day cycles (14 days total, purple), the Nyquist plot still overlaps closely with the previous measurements.

Due to the inherent technical challenges of independently measuring the impedance of the membrane and anode in a zero-gap cell configuration, we are unable to decouple the individual contributions from each component. Nevertheless, the absence of any appreciable change in the full-cell resistance throughout the entire testing period strongly suggests that both the membrane and the anode remain stable during prolonged dynamic operation and extended shutdown cycles. Further discussion has been added in the manuscript (Page 9, Supplementary Page 35)

Page 9:

Moreover, the stable of the full-cell resistance over the entire testing period strongly indicates that both the membrane and the anode remain stable during prolonged dynamic operation and extended shutdown cycles (Supplementary Fig. 34).

Supplementary Page 35:

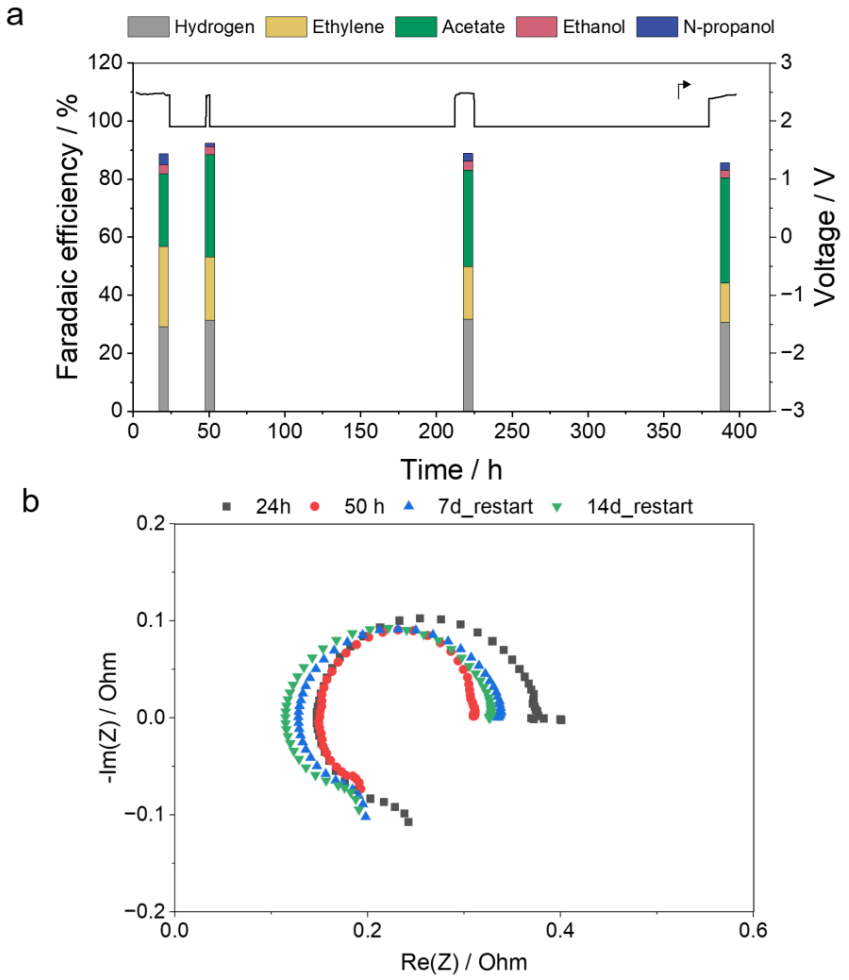

Supplementary Fig. 34 | Electrochemical impedance spectra of the CO electrolyzer at different stages of dynamic operation. **a |** Power-down operation at 1.9 V in CO for 7days two times**. b |** Nyquist plots collected after 24 h of initial stabilization (black), 50 h of operation (red), after the first 7-day power-down cycle (green), and after the second 7-day power-down cycle (purple) in Pannel a.

Specific Comment R2-7: *The authors employ a four-layer Cu (100) slab with the PBE-D3 functional and the CHEmethod to calculate the pathway, reporting both ΔG and ΔG‡. However, it is well known that the CHE approach and conventional*

constant-potential DFT carry inherent limitations when modeling charged interfaces, explicit solvent effects, and high OH^- concentrations (pH 14). Potential-dependent adsorption energies, solvation effects, and interfacial charge distributions can significantly affect both adsorption energetics and reaction barriers.

Response: We thank the reviewer for this valuable comment. In response, we performed grand-canonical DFT calculations on the Cu(100) surface to explicitly account for potential-dependent effects. Within the grand-canonical framework, all potential-dependent energetics, including interfacial charge redistribution, are inherently incorporated. Solvation effects were treated using an implicit solvent model.

Using this approach, we found that OH^- adsorption is significantly unfavorable at U > -0.05 V, which strongly influences the overall kinetics of carbonate formation. To quantify this effect, we combined the potential-dependent OH^- adsorption free energy with the CO*-OH* coupling barrier to estimate the effective kinetic barrier, and we further evaluated the corresponding turnover frequency of the reaction.

Notably, the predicted potential dependence shows excellent agreement with our experimental observations: carbonate poisoning readily occurs at open-circuit potential (OCP), whereas the application of a modest negative bias (−0.3 V vs. RHE) effectively suppresses carbonate formation and mitigates surface poisoning. These new results have been added to the main manuscript. (Page 7-8 and S12)

Page 6-8:

To further validate the proposed carbonate-poisoning mechanism, we performed DFT calculations. Supplementary Fig. 11 presents the free-energy landscapes for surface carbonate formation from $CO_{(aq)}$ on the Cu(100), (110), (111), and (310) facets at −0.07 V vs. RHE, corresponding to the OCP condition. Starting from adsorbed hydroxide (OH*) and carbon monoxide (CO*), their coupling to form the HO–CO bond requires an activation barrier ($\Delta G^{\ddagger}$) of 0.62 eV on (100), 0.73 eV on (110), 0.63 eV on (111), and 0.61 eV on (310). With the exception of the (110) facet, these barriers are comparable across the different surfaces. Once the OCOH* intermediate is formed, further oxidation to CO_2* requires additional free energy on the (110) and (111) facets (0.34 and 0.18 eV, respectively). In contrast, the (310) facet requires only 0.07 eV, while on the (100) surface OCOH* and CO_2* are thermodynamically near equilibrium. In addition to its favorable energetics for CO_2 formation from CO, the Cu(100) facet has been experimentally observed under *in-situ*/*operando* $CO_{(2)}$RR conditions.[27-32] Accordingly, we selected Cu(100) for a more detailed kinetic analysis.

To accurately capture the effect of surface charging under explicit electrochemical bias, we carried out grand-canonical DFT calculations on Cu(100).[33] Fig. 3a shows the grand-potential diagrams at −0.07 and −0.30 V vs. RHE. Once OCOH* is formed, subsequent $CO_{2(g)}$ generation, its conversion to carbonate, and carbonate adsorption are all thermodynamically favorable at both potentials. These results indicate that the formation of OCOH* from CO* and OH* constitutes the rate-determining step (RDS) for carbonate formation. While CO adsorption on Cu is thermodynamically favorable and largely insensitive to the applied potential, OH^- electrosorption exhibits a strong potential dependence. Accordingly, the effective kinetic barrier was evaluated as

$$\Delta G^{\ddagger}(U) = \max\left(0, \Delta G_{OH}^{ads}(U)\right) + \Delta G_{RDS}^{\ddagger}(U)$$

where the $\Delta G_{OH}^{ads}(U)$ is free energy for electrosorption of OH- ion and $\Delta G_{RDS}^{\ddagger}(U)$ is the activation barrier for OC*-OH* coupling to form OCOH* as a function of potential (U).

The potential-dependent $\Delta G^{\ddagger}$ for the RDS and the corresponding turnover frequency (ToF) are shown in Fig. 3b. $\Delta G^{\ddagger}$ decreases linearly with increasing potential and reaches a plateau at −0.05 V vs. RHE, where OH^- electrosorption becomes favorable—close to the OCP condition. The predicted ToF values for the RDS are 1.34 /s ($\Delta G^{\ddagger}$ = 0.75 eV) at −0.07 V vs. RHE and 7.57×10^{-7} /s ($\Delta G^{\ddagger}$ = 1.12 eV) at −0.30 V vs. RHE. These results clearly demonstrate that carbonate formation and the associated surface poisoning can readily occur under OCP conditions, whereas the application of a slightly negative potential effectively suppresses $CO_{2(g)}$ formation and, consequently, mitigates carbonate poisoning.

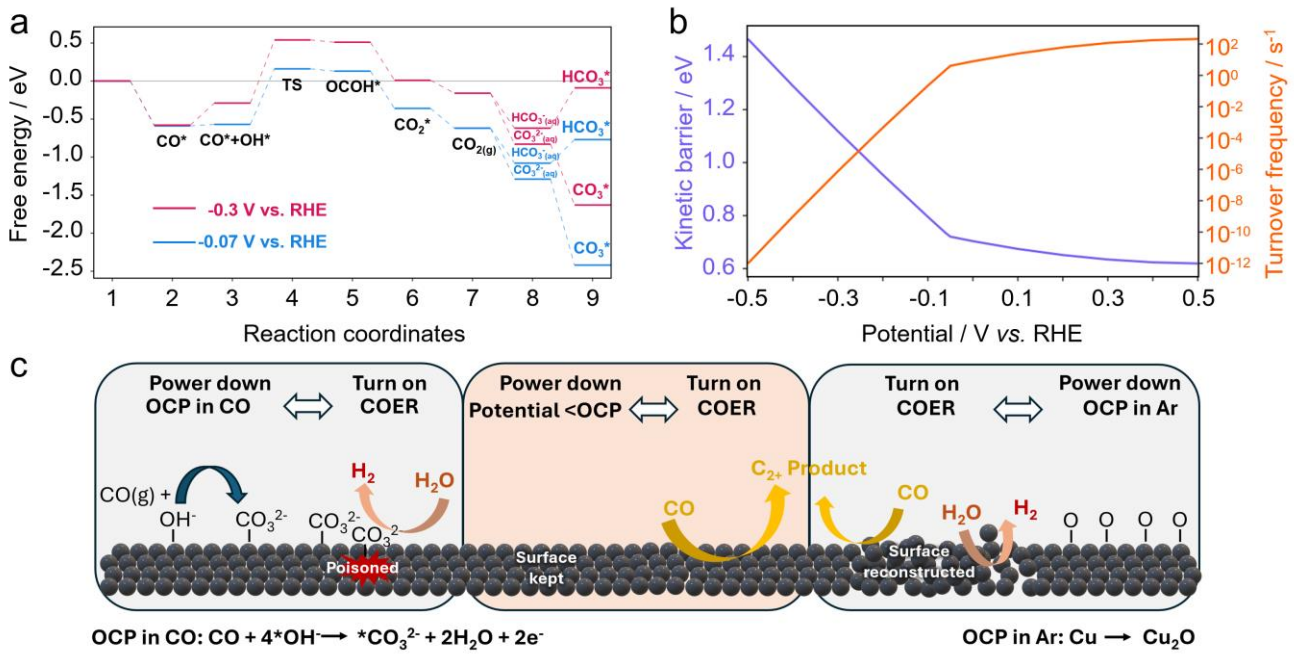

Fig. 3 | Mechanistic insights into catalyst state evolution during dynamic CO electroreduction. a | Grand canonical Density functional theory calculations – (Bi)carbonate formation on the copper surface. Free-energy landscape at 298K for the (bi)carbonate pathway from CO(aq) on Cu(100) at -0.07 V and -0.3 V vs. RHE. It shows that the OCOH* formation would be effectively suppressed by minimizing OH^- electrosoprtion. It also shows that CO_3* formation is energetically more favorable than HCO_3* formation. **b** | Total kinetic barrier and turnover frequency of OCOH* formation which is rate-determining step for (bi)carbonate formation. **c** | Schematic illustration of catalyst surface states during dynamic CO electroreduction operation. Under OCP in CO atmosphere (left), carbonate accumulation poisons the Cu surface. Under potential < OCP (middle), the surface remains active. Under OCP in Ar (right), the surface reconstructs to Cu2O due to oxidation.

Page S12:

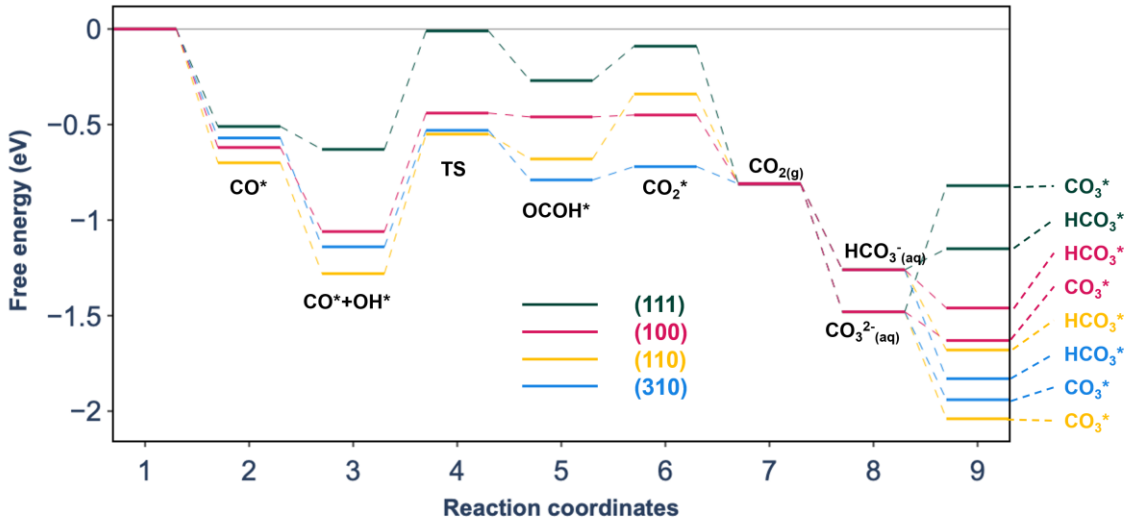

Supplementary Fig. 11 | Free energy landscape at -0.07 V vs. RHE at pH 14 on different facets of Cu.

Specific Comment R2-8: *The calculations are restricted to the Cu (100) surface, while other facets such as (111), (110), step/edge, and grain-boundary sites are neglected. These sites may exhibit distinct reaction pathways and barriers, as also suggested by experimental evidence indicating facetdependent responses. Although the authors briefly mention this possibility, no calculations were performed to substantiate it.*

Response: We thank the reviewer for this insightful comment. In response, we extended our DFT calculations to additional Cu facets, including Cu(110), Cu(111), and Cu(310), where the latter represents a stepped/edge-like surface. Grain-boundary sites were not considered, as they are not well defined in size for surface-reaction modeling within conventional slab-based DFT approaches.

Our results show that the Cu(100) and Cu(310) surfaces exhibit comparable energetics for CO-derived carbonate formation, whereas the Cu(110) and Cu(111) facets are significantly less favorable for CO_2 generation and subsequent carbonate formation. In particular, although the kinetic barrier for OCOH* formation on Cu(310) is similar to that on Cu(100), the subsequent deprotonation of OCOH* to form CO_2* requires a slightly higher free energy on Cu(310).

Based on these results, we focused our grand-canonical DFT analysis on the Cu(100) surface as a representative and kinetically relevant facet. In addition, we have included further rich references supporting the preferential formation and stabilization of Cu(100) facets under CO_2RR operating conditions.

This new result is also described in the first part of DFT section in the main manuscript. (Page 7-8 and S12)

Specific Comment R2-9: *The manuscript contains careless omissions of units. For example, the sentence "The subsequent electrosorption of $CO3^{2-}$(aq) releases an energy of ΔG = -1.13" lacks the unit of ΔG. The authors must carefully check the entire manuscript (main text, figures, tables and Supporting Information) and correct all instances where physical/chemical quantities are missing units.*

Response: We thank the reviewer for pointing out this oversight. We have carefully re-examined the entire manuscript, including the main text, figures, tables, and Supplementary Information, to ensure that all physical and chemical quantities are reported with proper units. Specifically, the Gibbs free energy (ΔG) mentioned in the text has been corrected to ΔG = –1.13 eV, and similar unit omissions throughout the paper have been systematically addressed.

Reviewer: 3

General Comments R3: *The manuscript discusses the dynamic operation of electrochemical CO conversion to C2+ chemicals. It combines experimental investigations with molecular simulation and technoeconomic analysis to argue that dynamic operation is possible without significant catalyst degradation by applying a power-down strategy that holds the potential at values below the open circuit potential, thus inhibiting carbonate and oxide formation.*

There is much merit in investigating the dynamic operation potential of electrochemical processes, especially because the premise often is they can operate economically feasibly when using renewable power (while infeasibly when using high C grid power) and/or switch off when spot market prices are high. We know from experience this is easier said than done, and developing suitable dynamic operating strategies for electrochemical devices is thus imperative.

I believe the main contribution of this manuscript is in the experimental evaluation, which to my mind is sound, but by itself will not justify publication in Nature Catalysis. I cannot comment on the DFT (I don't have the expertise) but the TEA appears very crude and does not compare to the quality of TEAs I've previously endorsed for publication in Nature titles.

If the authors are willing to make a significant effort to improve the TEA, I'd be happy to reconsider the manuscript. Here's some guidance:

The key weakness is the sparse selection of cases - rendering the insights very specific while not allowing to draw generalisable insights - and the sheer lack of methodological information (both in the methods and in the SI).

Response: We thank the reviewer for the positive feedback and thoughtful suggestions. We have addressed all concerns as follows:

Specific Comment R3-1: *To point 1: I understand why grid prices in Southern Australia are included - and cross referenced with Norway - but the authors will agree the selection of locations is minimal. To allow generalisability, I'd include at least 10 locations across the globe that span the envelope of possible renewable energy performance. Also, I'd look at including all 4 seasons (for countries where there are 4, otherwise select as appropriate) to include the fluctuations in renewable energy production throughout a year, plus, please don't use the values from 1 day, but take an average electricity price profile over a month (or even better evaluate the performance for each day in the month selected). Try to synthesise learning from this analysis, including on what this could mean for the number of starts/stops in a day/week/month/year, and how this reflects on the cathode performance observed.*

Response: We appreciate the reviewer's valuable comment. We have now included 10 different countries (United States, Chile, Norway, Denmark, Spain, France, Germany, Hungary, Japan, and Australia) in a four-season analysis, in addition to the South Australia case. We found a strong positive correlation between the standard deviation of electricity price and the potential acetic acid production cost saving from dynamic operation. The results are described in both the main text (pages 11-12, Fig. 5) and the Supplementary Information (Supplementary Fig. 41 and 44-53, Supplementary Tables 3-10).

Pages 11-12:

Varying the operational capacity and corresponding electricity prices, as well as the standard deviation of electricity prices, significantly affect acetic acid production costs (Fig. 5). We compared the cases of South Australia and Norway, representing intermittent renewable energy with high electricity price variability and non-intermittent renewable energy with low variability, respectively (Fig. 5a). For South Australia, where intermittent renewable energy sources are utilized, operating at 50% capacity yielded the lowest production cost at 1.34 USD kg^{-1}, representing a 32% cost saving relative to the full capacity cost of 1.96 USD kg^{-1} by avoiding peak electricity prices (Fig. 5a, Supplementary Fig. 41a). Even operation at 25% capacity resulted in a 23% cost saving (1.51 USD kg^{-1}) compared to full capacity, due to the high contribution of electricity costs for the electrolyzer at full capacity, which accounted for more than 56% of the overall cost (Supplementary Fig. 41a). Operating at 50% capacity enabled production cost savings by utilizing low-cost electricity while reducing the capital expense

contribution to 16% of the overall cost (Supplementary Fig. 41a). The electricity used during the power-down period remained less than 1% of production cost for various operating capacities (Supplementary Fig. 41a).

For regions powered by steady renewable energy sources, such as hydropower and geothermal energy, electricity prices tend to be more stable. In Norway, over 98% of electricity generation comes from renewable sources, with hydropower accounting for 89% and wind energy for 9% (Supplementary Fig. 42).[45] When the TEA was conducted using hourly weekday electricity prices from June to August 2024, averaging 0.03 USD kWh^{-1} with a low standard deviation of 0.004 USD kWh^{-1} (Supplementary Fig. 43)[46], steady state operation resulted in the lowest production cost at 0.765 USD kg^{-1} (Fig. 5a). This is because the low standard deviation in electricity price does not substantially increase the electricity cost contribution to acetic acid production as capacity increases (28–33% at capacities from 62.5% to 100%), while the capital expenditure proportion decreases below 14% at 100% capacity (Supplementary Fig. 41b).

Since electricity costs for the electrolyzer account for about half of the production cost[14] (Supplementary Fig. 40), the electricity price input is a critical factor in determining whether dynamic operation is more economical. We calculated the acetic acid production cost at varying operational capacities for 10 countries worldwide (Fig. 5b, Supplementary Fig. 44 – 53, Supplementary Table. 3 – 10), for which hourly electricity price data are available on the IEA website to enable a fair comparison. Four seasons – spring, summer, fall, and winter – were considered for each country in the analysis. The standard deviation of the electricity prices shows a strong positive correlation with acetic acid production cost savings, with an R^2 value of 0.945 when Chile is excluded (Fig. 5b; with Chile included, R^2 = 0.889). Chile appears as an outlier because its hourly electricity price scheme is distinct from those of other countries, exhibiting a binary-like pattern in the hourly electricity price curve (Supplementary Fig. 45 (a, c, e, g)). These results demonstrate that a higher standard deviation in electricity price leads to greater acetic acid production cost savings under dynamic operation, and that the standard deviation can be used as a metric to determine whether dynamic operation or steady state operation is more economically favorable. By designing the facility for full capacity (50,000 kg day^{-1} in this analysis), operation can be adjusted to run either intermittently or continuously in response to daily electricity price fluctuations, thus offering greater flexibility than a system sized strictly for lower-capacity operation. It should be noted that this TEA focuses on production costs and does not account for the market demand and supply.

These TEA results highlight the importance of dynamic operation for the economic viability of CO electrolysis and the benefits of accessing lower electricity prices. Depending on the standard deviation of electricity prices, operators can adjust the operating mode, choosing either intermittent or steady state operation, to reduce production costs.

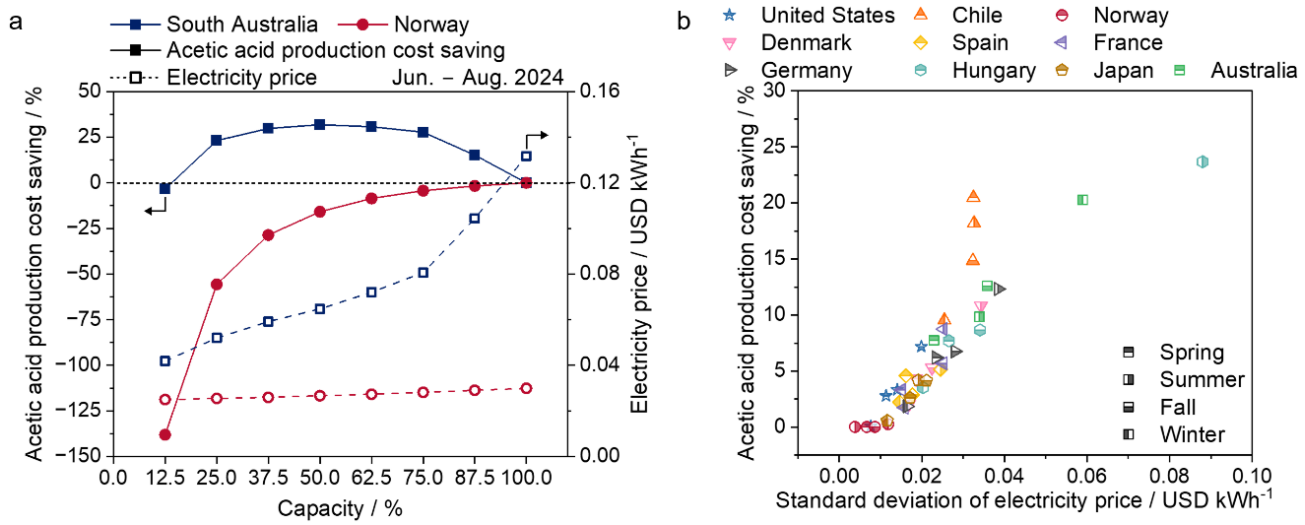

Fig. 5 | Techno-economic analysis of dynamic and steady state operation of CO electrolyzers for acetic acid production. a | Comparison of South Australia (intermittent renewables, high standard deviation in electricity price: 0.097 USD kWh^{-1}) and Norway (non-intermittent renewables, low standard deviation in electricity price: 0.004 USD kWh^{-1}). The left y-axis shows the acetic acid production cost saving relative to 100% capacity (with 100% capacity corresponding to 50,000 kg day^{-1}), while the right y-axis displays the corresponding weekday electricity price in South Australia[44] and Norway from June to August 2024[46].

b | Acetic acid production cost saving as a function of the standard deviation of electricity price for 10 countries worldwide, evaluated across four seasons (spring, summer, fall, and winter) from September 2023 to August 2024.

Page S42:

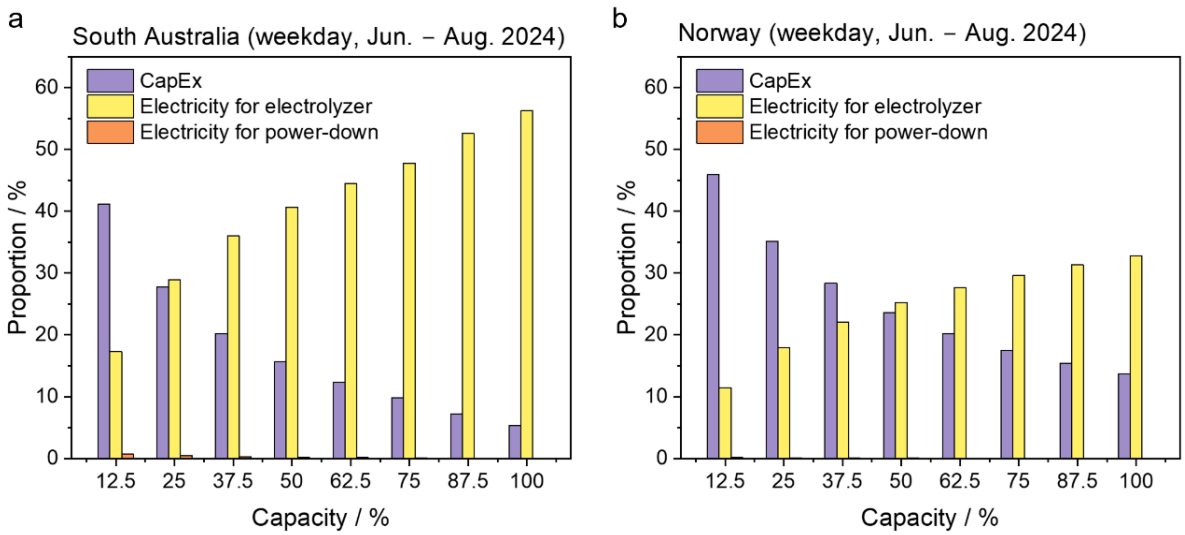

Supplementary Fig. 41 | CapEx proportion and electricity for electrolyzer proportion for acetic acid production from CO electrolyzers in South Australia (a) and Norway (b) from June to August 2024. The acetic acid production cost saving relative to 100% capacity is shown in Fig. 5a.

Pages S45-54:

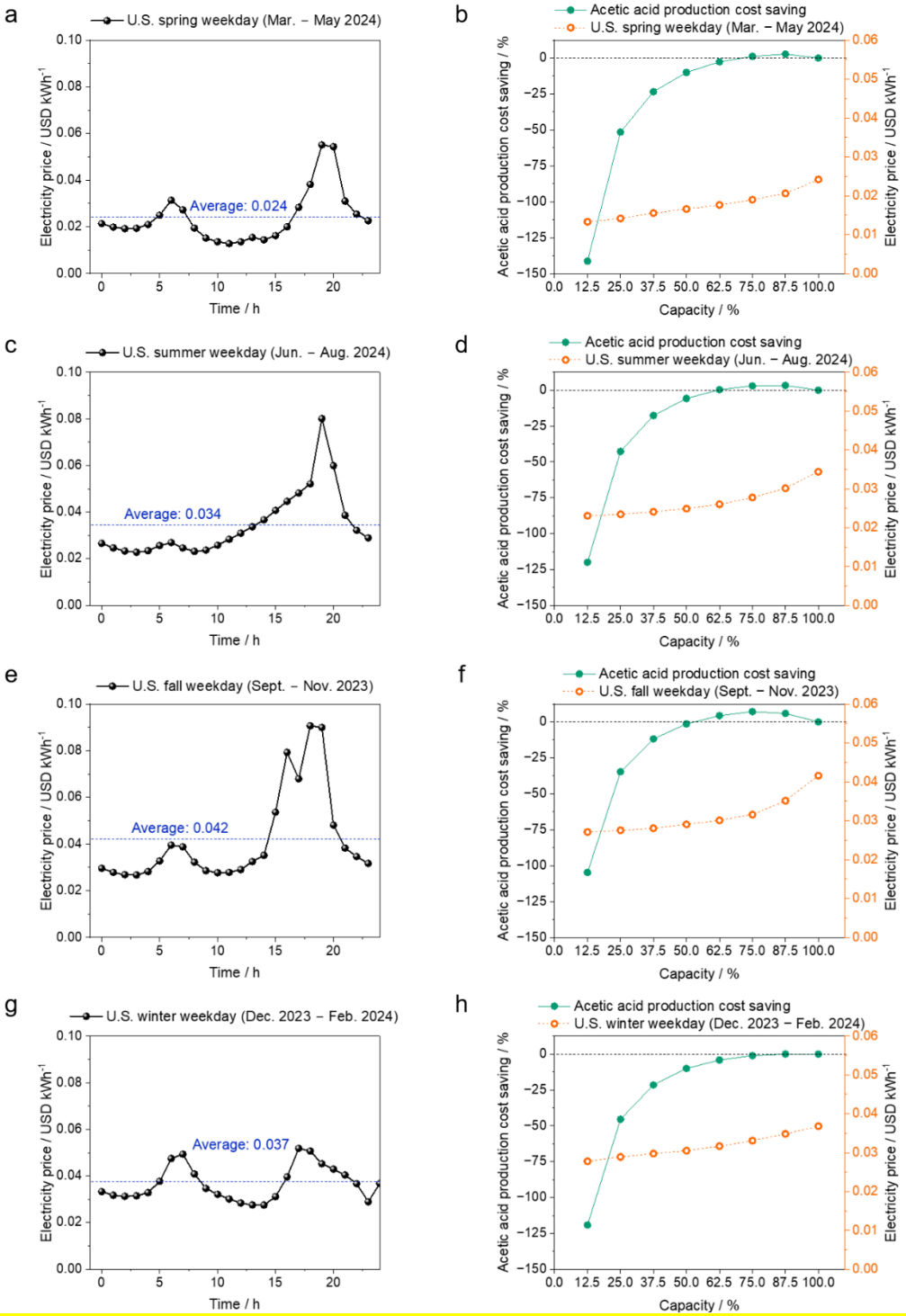

Supplementary Fig. 44 | Hourly averaged weekday electricity prices (a, c, e, g)[13-16] and the corresponding techno-economic analysis of dynamic and steady state operation of CO electrolyzers for acetic acid production (b, d, f, h) in the United States from September 2023 to August 2024. Acetic acid production cost savings are plotted relative to operation at 100% capacity.

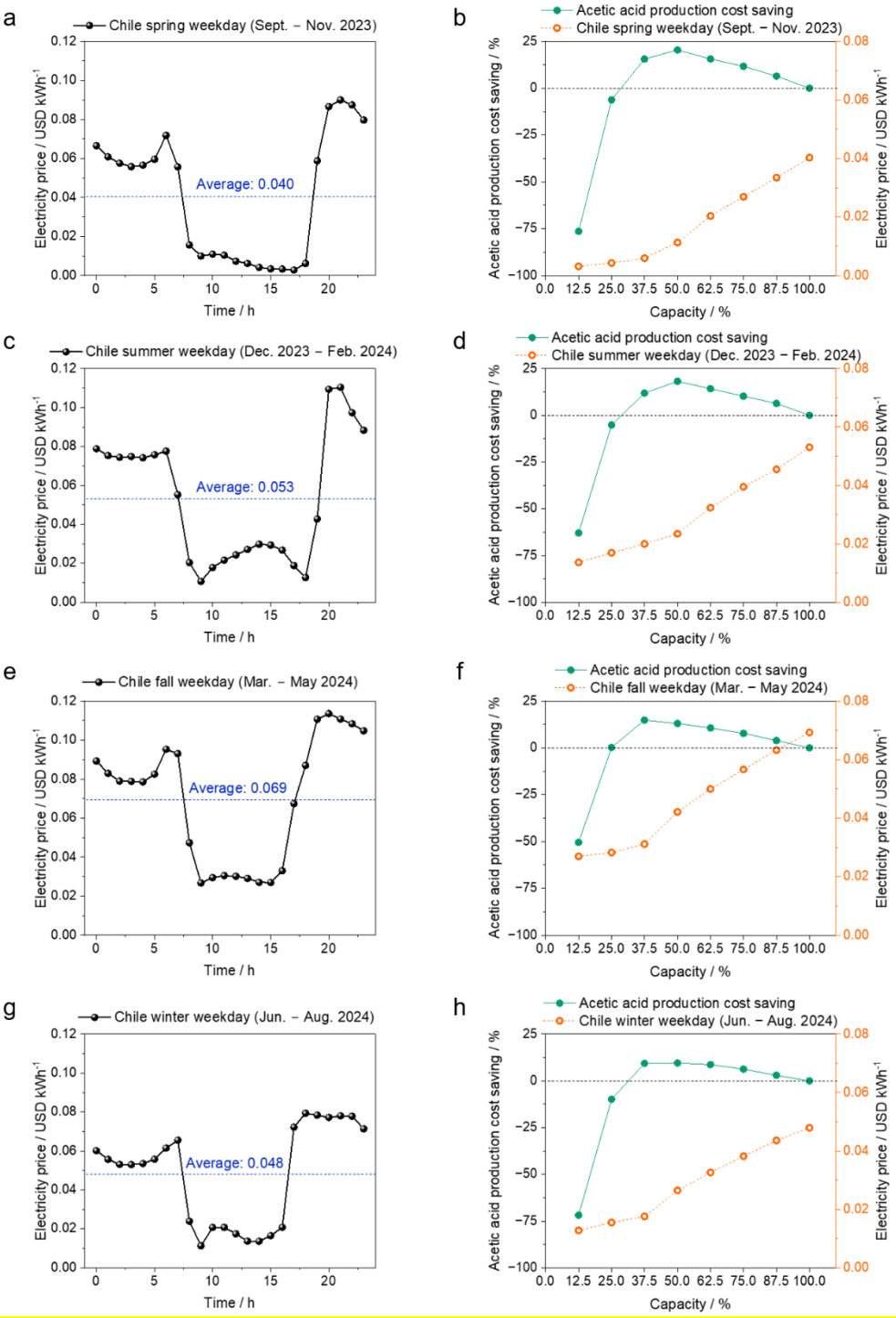

Supplementary Fig. 45 | Hourly averaged weekday electricity prices (a, c, e, g)[17-20] and the corresponding techno-economic analysis of dynamic and steady state operation of CO electrolyzers for acetic acid production (b, d, f, h) in Chile from September 2023 to August 2024. Acetic acid production cost savings are plotted relative to operation at 100% capacity.

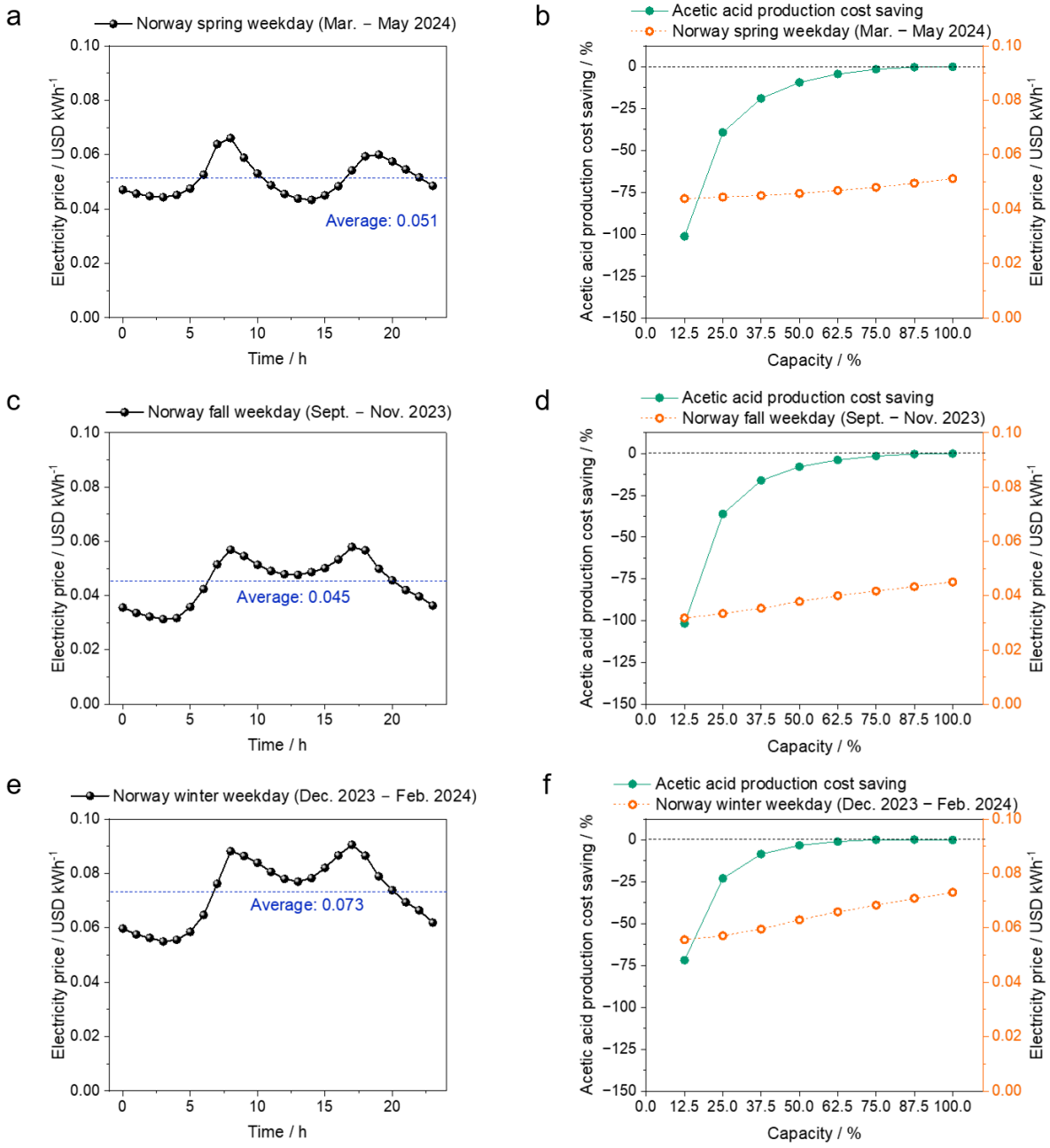

Supplementary Fig. 46 | Hourly averaged weekday electricity prices (a, c, e)[21-23] and the corresponding techno-economic analysis of dynamic and steady state operation of CO electrolyzers for acetic acid production (b, d, f) in Norway from September 2023 to May 2024. Acetic acid production cost savings are plotted relative to operation at 100% capacity. For summer (June – August 2024), the hourly averaged weekday electricity price is shown in Supplementary Fig. 42, and the corresponding techno-economic analysis is shown in Fig. 5a.

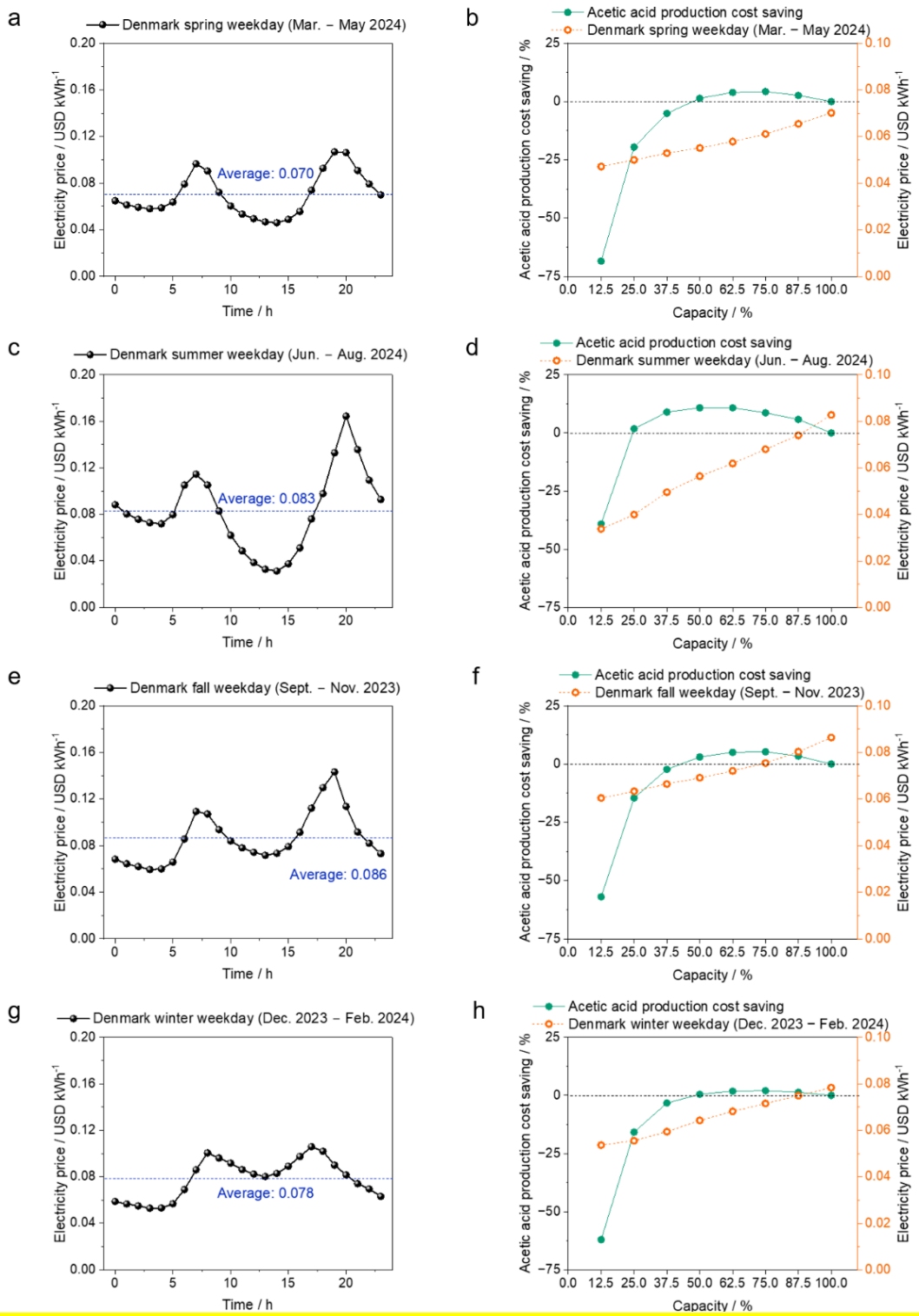

Supplementary Fig. 47 | Hourly averaged weekday electricity prices (a, c, e, g)[24-27] and the corresponding techno-economic analysis of dynamic and steady state operation of CO electrolyzers for acetic acid production (b, d, f, h) in Denmark from September 2023 to August 2024. Acetic acid production cost savings are plotted relative to operation at 100% capacity.

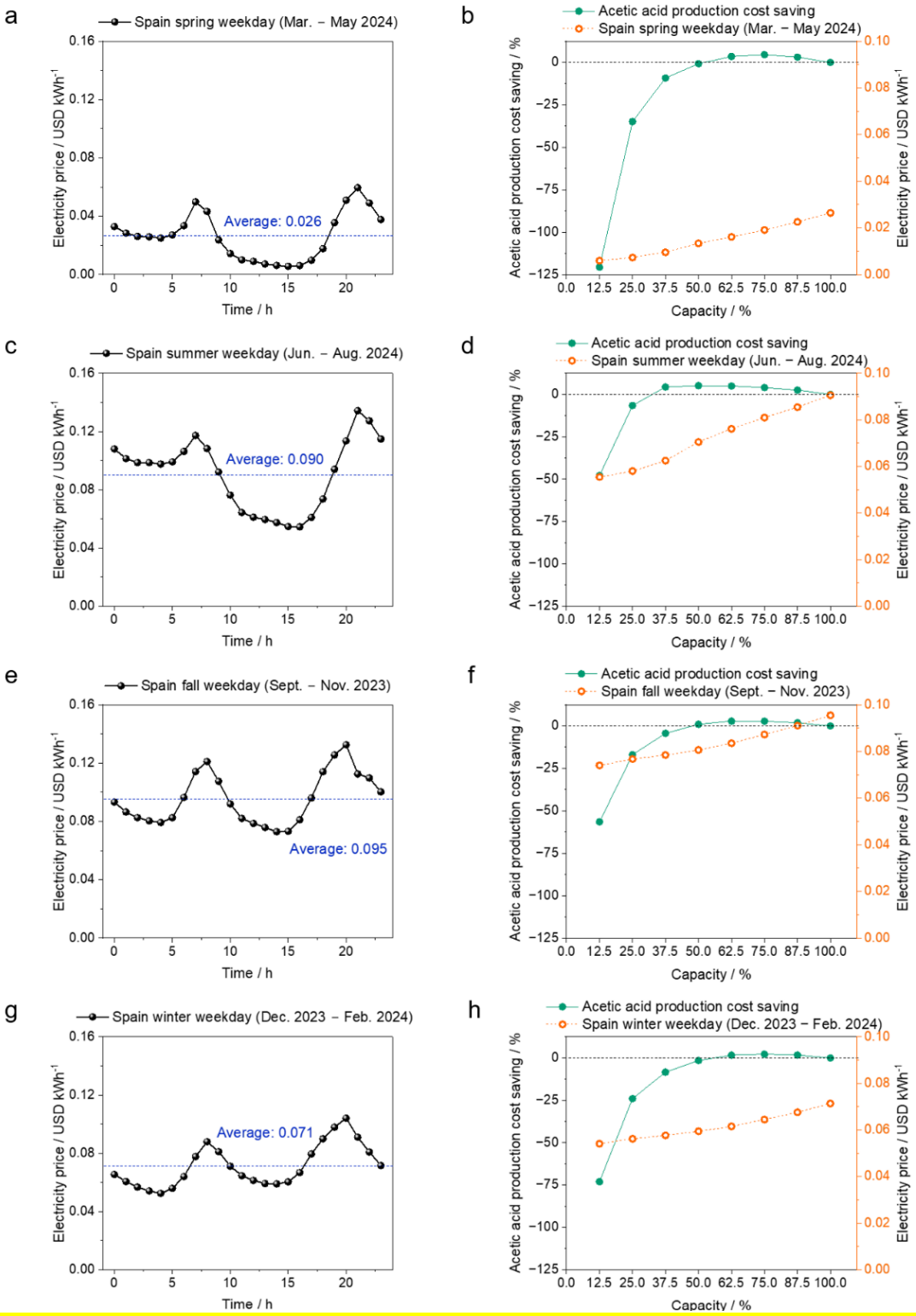

Supplementary Fig. 48 | Hourly averaged weekday electricity prices (a, c, e, g)[28-31] and the corresponding techno-economic analysis of dynamic and steady state operation of CO electrolyzers for acetic acid production (b, d, f, h) in Spain from September 2023 to August 2024. Acetic acid production cost savings are plotted relative to operation at 100% capacity.

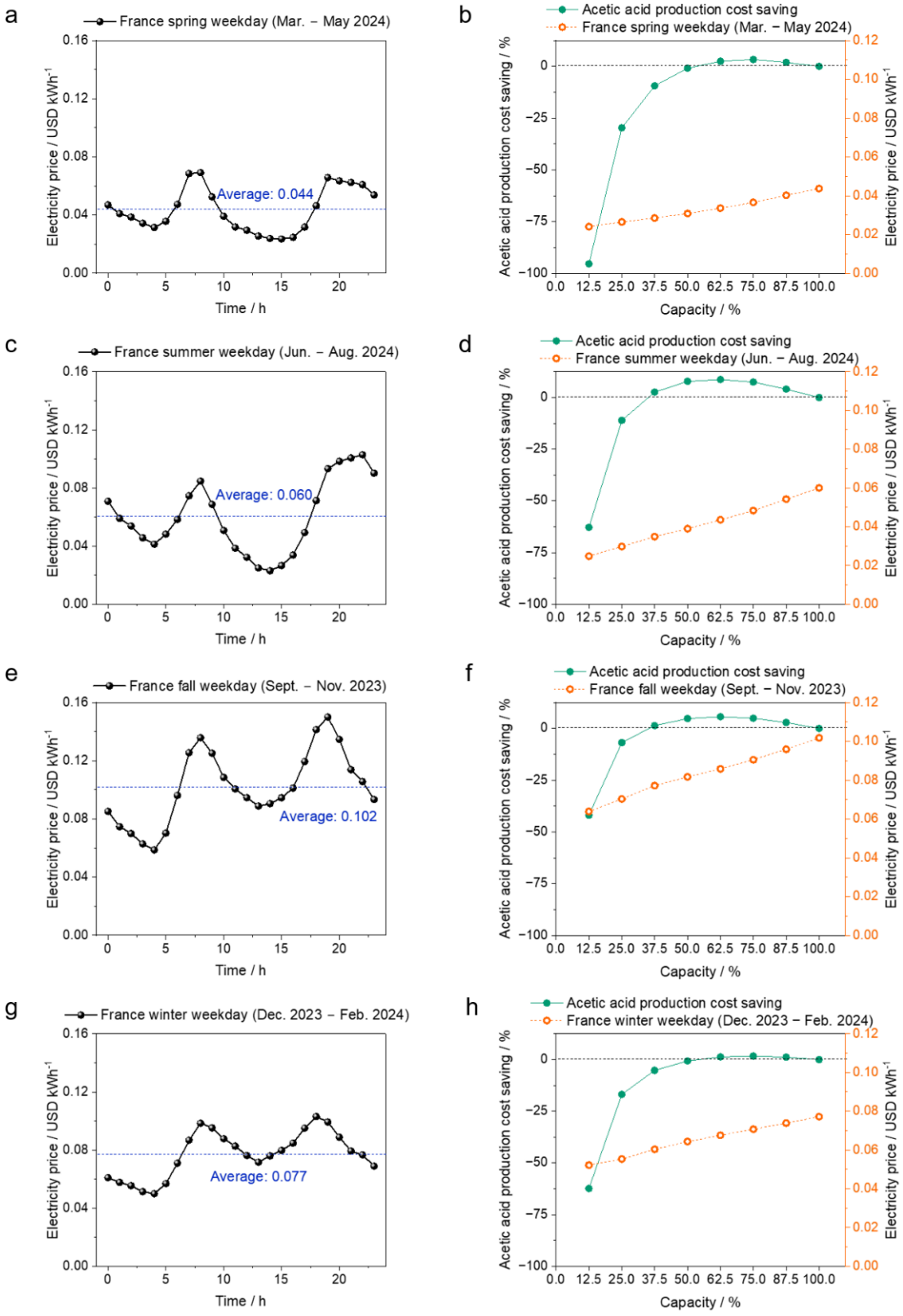

Supplementary Fig. 49 | Hourly averaged weekday electricity prices (a, c, e, g)[32-35] and the corresponding techno-economic analysis of dynamic and steady state operation of CO electrolyzers for acetic acid production (b, d, f, h) in France from September 2023 to August 2024. Acetic acid production cost savings are plotted relative to operation at 100% capacity.

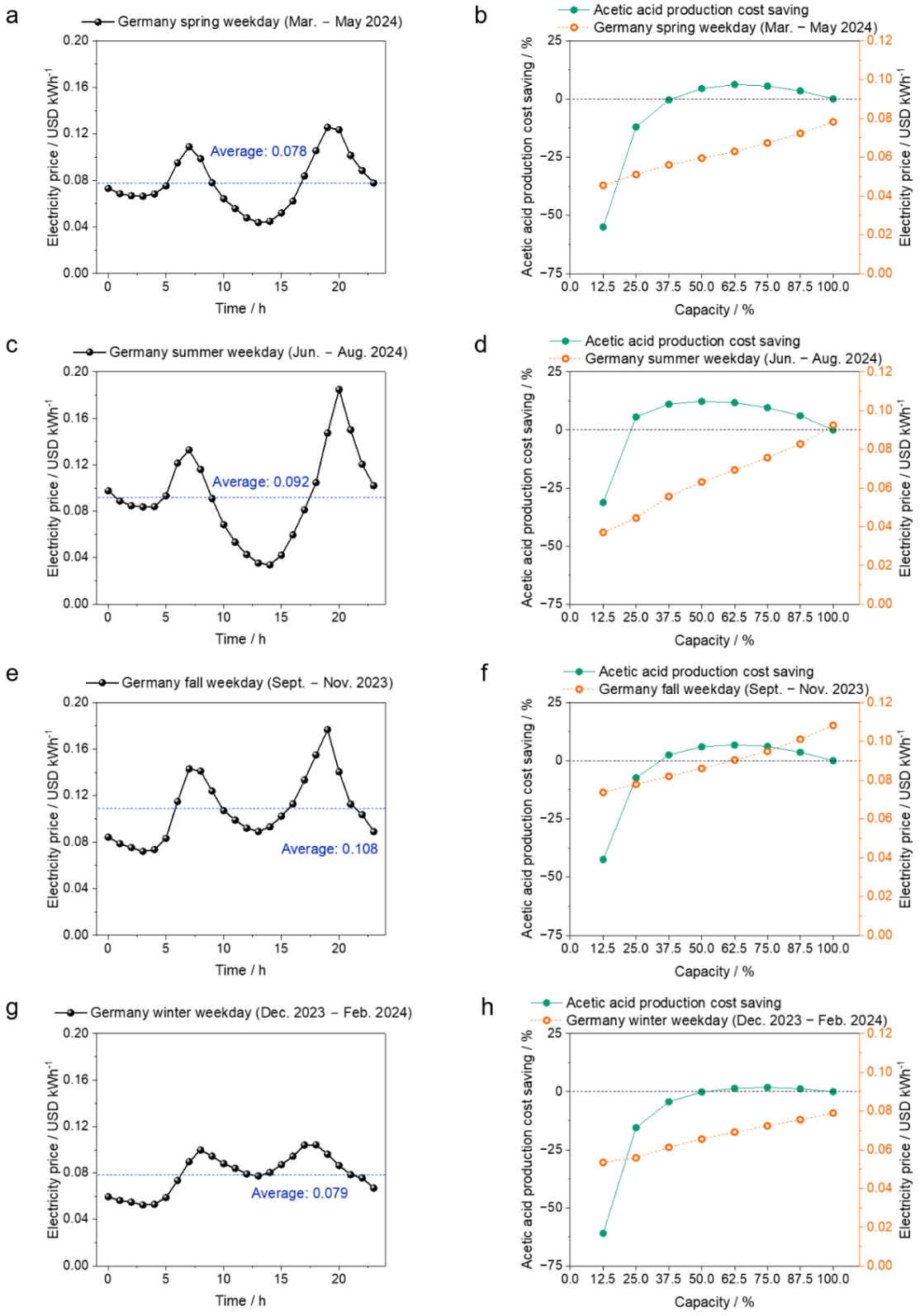

Supplementary Fig. 50 | Hourly averaged weekday electricity prices (a, c, e, g)[36-39] and the corresponding techno-economic analysis of dynamic and steady state operation of CO electrolyzers for acetic acid production (b, d, f, h) in Germany from September 2023 to August 2024. Acetic acid production cost savings are plotted relative to operation at 100% capacity.

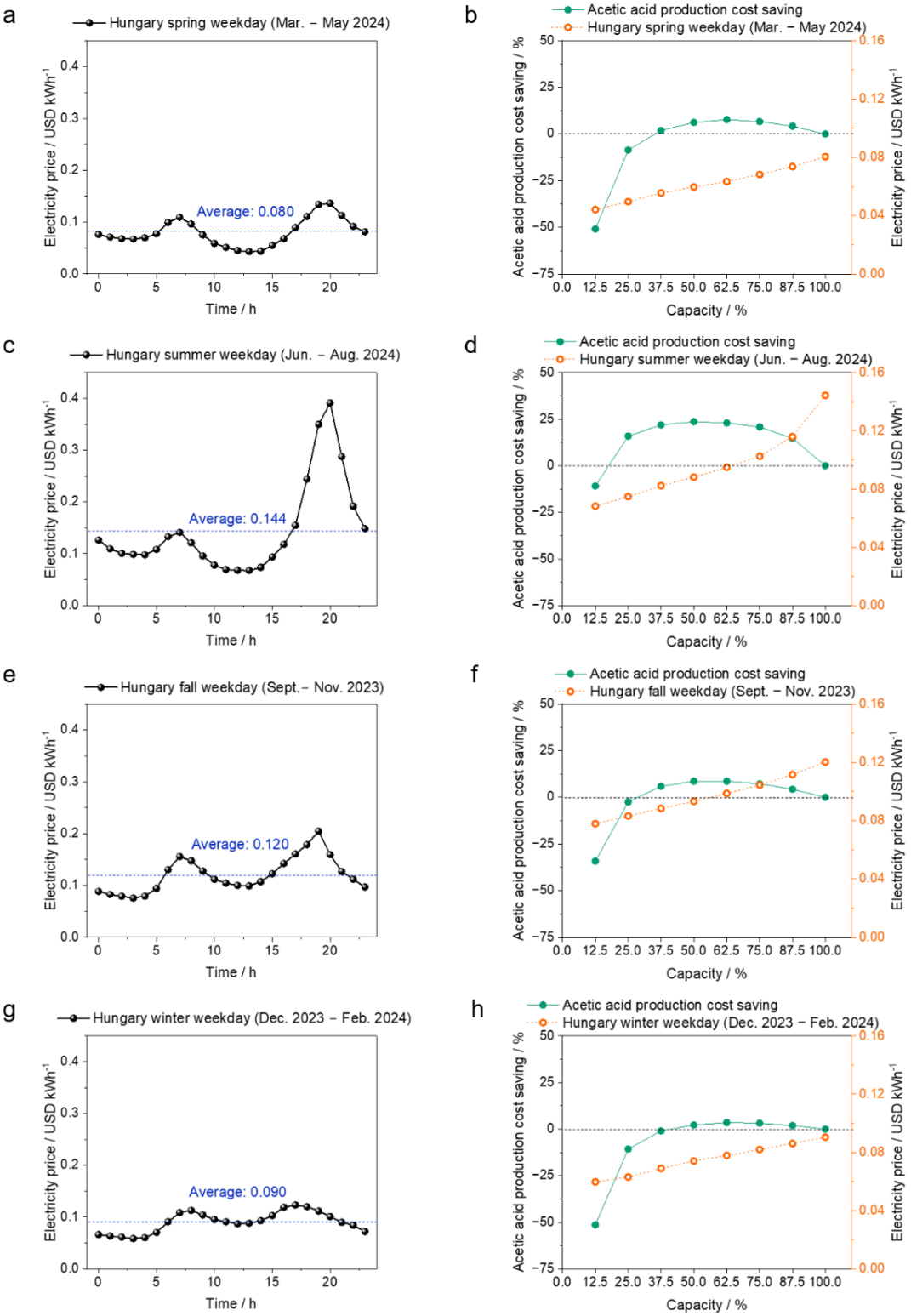

Supplementary Fig. 51 | Hourly averaged weekday electricity prices (a, c, e, g)[40-43] and the corresponding techno-economic analysis of dynamic and steady state operation of CO electrolyzers for acetic acid production (b, d, f, h) in Hungary from September 2023 to August 2024. Acetic acid production cost savings are plotted relative to operation at 100% capacity.

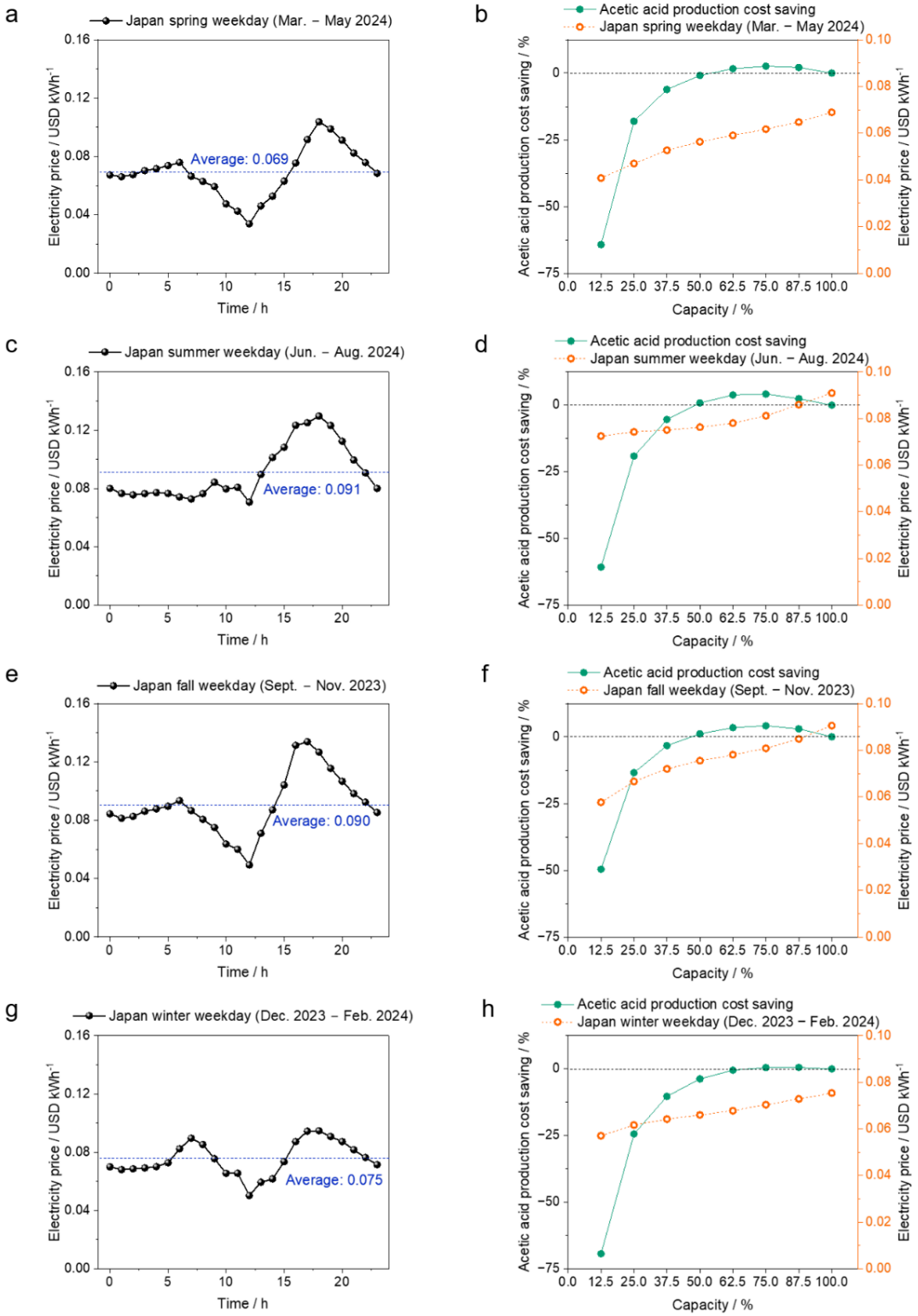

Supplementary Fig. 52 | Hourly averaged weekday electricity prices (a, c, e, g)[44-47] and the corresponding techno-economic analysis of dynamic and steady state operation of CO electrolyzers for acetic acid production (b, d, f, h) in Japan from September 2023 to August 2024. Acetic acid production cost savings are plotted relative to operation at 100% capacity.

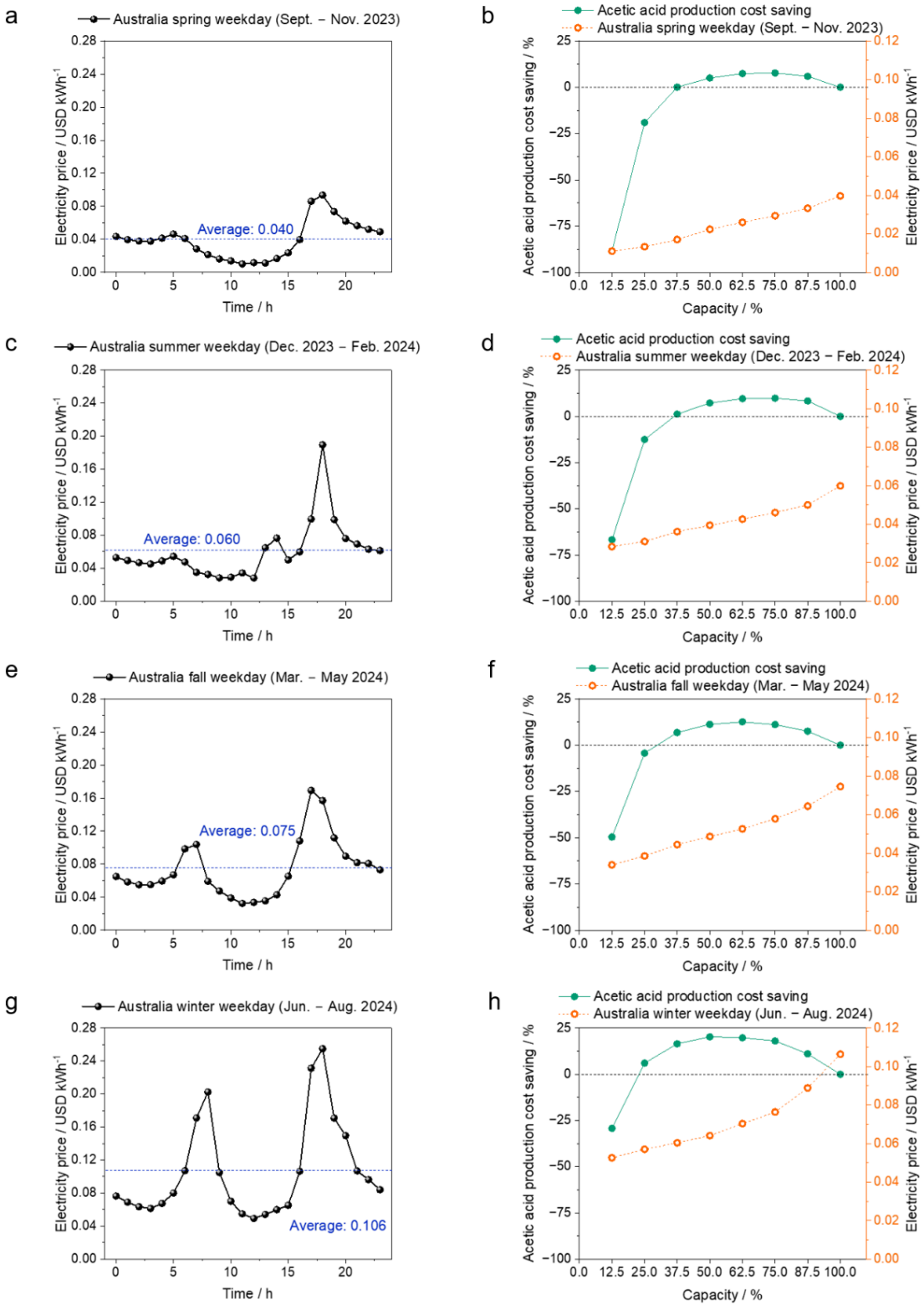

Supplementary Fig. 53 | Hourly averaged weekday electricity prices (a, c, e, g)[48-51] and the corresponding techno-economic analysis of dynamic and steady state operation of CO electrolyzers for acetic acid production (b, d, f, h) in Australia from September 2023 to August 2024. Acetic acid production cost savings are plotted relative to operation at 100% capacity.

Pages S60-63:

Supplementary Table 3 | Acetic acid production cost savings at each capacity and the production cost at 100% capacity for 10 countries in spring. For Australia and Chile, hourly weekday electricity prices from September to November 2023 were used, while for other countries, hourly weekday electricity prices from March to May 2024 were used. The most cost-effective cases are shown in bold.

Spring (September – November 2023 for Australia and Chile | March – May 2024 for other countries)										
Acetic acid production cost saving (%)										
	North America	South America	Europe						Asia	Oceania
Capacity (%)	United States	Chile	Norway	Denmark	Spain	France	Germany	Hungary	Japan	Australia
12.5	-141.3	-76.4	-101.3	-68.4	-120.6	-95.4	-55.0	-50.8	-64.2	-88.4
25	-51.5	-6.2	-39.2	-19.5	-34.9	-29.7	-12.0	-8.5	-18.0	-19.0
37.5	-23.4	15.6	-18.9	-5.1	-9.2	-9.4	-0.4	1.9	-6.1	0.1
50	-10.0	**20.5**	-9.4	1.4	-0.8	-0.9	4.5	6.2	-0.9	5.0
62.5	-2.6	15.6	-4.3	3.9	3.5	2.4	**6.2**	**7.7**	1.7	7.4
75	1.1	11.7	-1.5	**4.3**	**4.6**	**3.3**	5.5	6.6	**2.6**	**7.7**
87.5	**2.8**	6.5	-0.2	2.6	3.1	1.9	3.5	4.2	2.1	5.9
100	0.0	0.0	**0.0**	0.0	0.0	0.0	0.0	0.0	0.0	0.0
Capacity (%)	Acetic acid production cost at 100% capacity (USD kg^{-1})									
100	0.698	0.888	1.017	1.239	0.725	0.928	1.334	1.361	1.225	0.881

Supplementary Table 4 | Acetic acid production cost savings at each capacity and the production cost at 100% capacity for 10 countries in summer. For Australia and Chile, hourly weekday electricity prices from December 2023 to February 2024 were used, while for other countries, hourly weekday electricity prices from June to August 2024 were used. The most cost-effective cases are shown in bold.

Summer (December 2023 – February 2024 for Australia and Chile | June – August 2024 for other countries)										
Acetic acid production cost saving (%)										
	North America	South America	Europe						Asia	Oceania
Capacity (%)	United States	Chile	Norway	Denmark	Spain	France	Germany	Hungary	Japan	Australia
12.5	-120.0	-63.0	-138.1	-39.1	-47.8	-62.8	-31.2	-10.9	-60.8	-66.7
25	-42.7	-5.2	-55.6	1.8	-6.6	-11.0	5.6	15.9	-19.1	-12.4
37.5	-17.6	11.9	-28.6	9.0	4.3	2.6	11.1	21.9	-5.4	1.2
50	-5.8	**18.2**	-15.8	**10.8**	**5.1**	7.9	**12.3**	**23.6**	0.8	7.3
62.5	0.3	14.2	-8.5	10.8	5.0	**8.7**	11.7	23.0	3.8	9.6
75	3.0	10.2	-4.3	8.7	4.0	7.5	9.6	20.8	**4.2**	**9.8**
87.5	**3.3**	6.3	-1.7	5.8	2.5	4.1	6.1	14.7	2.4	8.4
100	0.0	0.0	**0.0**	0.0	0.0	0.0	0.0	0.0	0.0	0.0
Capacity (%)	Acetic acid production cost at 100% capacity (USD kg^{-1})									
100	0.818	1.038	0.765	1.388	1.480	1.120	1.503	2.114	1.485	1.119

Supplementary Table 5 | Acetic acid production cost savings at each capacity and the production cost at 100% capacity for 10 countries in fall. For Australia and Chile, hourly weekday electricity prices from March to May 2024 were used, while for other countries, hourly weekday electricity prices from September to November 2023 were used. The most cost-effective cases are shown in bold.

Fall (March – May 2024 for Australia and Chile | September – November 2023 for other countries)										
Acetic acid production cost saving (%)										
	North America	South America	Europe						Asia	Oceania
Capacity (%)	United States	Chile	Norway	Denmark	Spain	France	Germany	Hungary	Japan	Australia
12.5	-104.7	-50.5	-101.6	-57.0	-56.5	-41.9	-42.4	-34.2	-49.6	-49.6
25	-34.7	0.3	-36.1	-14.6	-16.9	-6.9	-7.4	-2.5	-13.4	-4.3
37.5	-11.8	**14.8**	-16.1	-2.3	-4.4	1.4	2.5	5.9	-3.3	6.8
50	-1.4	13.0	-7.9	3.0	0.9	4.7	6.0	**8.6**	1.1	11.3
62.5	4.4	10.7	-3.8	5.0	**2.9**	**5.7**	**6.7**	8.6	3.5	**12.6**
75	**7.2**	7.8	-1.4	**5.3**	2.8	4.9	6.2	7.2	**4.1**	11.1
87.5	5.9	3.9	-0.3	3.4	1.9	2.8	3.6	4.4	3.0	7.5
100	0.0	0.0	**0.0**	0.0	0.0	0.0	0.0	0.0	0.0	0.0
Capacity (%)	Acetic acid production cost at 100% capacity (USD kg^{-1})									
100	0.903	1.229	0.944	1.430	1.537	1.612	1.688	1.830	1.480	1.292

Supplementary Table 6 | Acetic acid production cost savings at each capacity and the production cost at 100% capacity for 10 countries in winter. For Australia and Chile, hourly weekday electricity prices from June to August 2024 were used, while for other countries, hourly weekday electricity prices from December 2023 to February 2024 were used. The most cost-effective cases are shown in bold.

Winter (June – August 2024 for Australia and Chile | December 2023 – February 2024 for other countries)										
Acetic acid production cost saving (%)										
	North America	South America	Europe						Asia	Oceania
Capacity (%)	United States	Chile	Norway	Denmark	Spain	France	Germany	Hungary	Japan	Australia
12.5	-119.2	-71.8	-71.8	-62.0	-73.0	-62.4	-61.0	-51.4	-69.4	-29.3
25	-45.5	-9.9	-23.0	-15.8	-24.0	-16.8	-15.4	-10.7	-24.4	6.1
37.5	-21.6	9.4	-8.5	-3.3	-8.4	-5.2	-4.3	-1.0	-10.3	16.5
50	-10.1	**9.5**	-3.2	0.5	-1.6	-0.6	-0.1	2.2	-3.7	20.3
62.5	-4.1	8.7	-1.0	1.8	1.6	1.3	1.5	**3.5**	-0.5	19.7
75	-1.1	6.3	0.1	**2.1**	**2.2**	**1.7**	**1.8**	3.1	0.5	18.0
87.5	**0.1**	2.9	**0.2**	1.4	1.7	1.2	1.3	1.9	**0.6**	11.0
100	0.0	0.0	0.0	0.0	0.0	0.0	0.0	0.0	0.0	0.0
Capacity (%)	Acetic acid production cost at 100% capacity (USD kg^{-1})									
100	0.847	0.978	**1.273**	1.336	1.253	1.323	1.344	1.478	1.301	1.667

Supplementary Table 7 | Maximum acetic acid production cost saving at the corresponding capacity and the production cost at that capacity for 10 countries in spring. For Australia and Chile, hourly weekday electricity prices from September to November 2023 were used, while for other countries, hourly weekday electricity prices from March to May 2024 were used. The average electricity price and its standard deviation for this period are shown for each country.

Spring (September – November 2023 for Australia and Chile | March – May 2024 for other countries)						
		Capacity (%)	Acetic acid production cost saving (%)	Corresponding acetic acid production cost (USD kg^{-1})	Average electricity price (USD kWh^{-1})	Standard deviation of electricity price (USD kWh^{-1})
North America	United States	87.5	2.8	0.679	0.024	0.011
South America	Chile	50	20.5	0.706	0.040	0.033
Europe	Norway	100	0.0	1.017	0.051	0.007
	Denmark	75	4.3	1.186	0.070	0.019
	Spain	75	4.6	0.692	0.026	0.016
	France	75	3.3	0.897	0.044	0.015
	Germany	62.5	6.2	1.252	0.078	0.024
	Hungary	62.5	7.7	1.256	0.080	0.027
Asia	Japan	75	2.6	1.194	0.069	0.017
Oceania	Australia	75	7.7	0.813	0.040	0.023

Supplementary Table 8 | Maximum acetic acid production cost saving at the corresponding capacity and the production cost at that capacity for 10 countries in summer. For Australia and Chile, hourly weekday electricity prices from December 2023 to February 2024 were used, while for other countries, hourly weekday electricity prices from June to August 2024 were used. The average electricity price and its standard deviation for this period are shown for each country.

Summer (December 2023 – February 2024 for Australia and Chile | June – August 2024 for other countries)						
		Capacity (%)	Acetic acid production cost saving (%)	Corresponding acetic acid production cost (USD kg^{-1})	Average electricity price (USD kWh^{-1})	Standard deviation of electricity price (USD kWh^{-1})
North America	United States	87.5	3.3	0.791	0.034	0.014
South America	Chile	50	18.2	0.849	0.053	0.033
Europe	Norway	100	0.0	0.765	0.030	0.004
	Denmark	50	10.8	1.238	0.083	0.034
	Spain	50	5.1	1.404	0.091	0.025
	France	62.5	8.7	1.022	0.060	0.025
	Germany	50	12.3	1.318	0.092	0.039
	Hungary	50	23.6	1.614	0.144	0.088
Asia	Japan	75	4.2	1.423	0.091	0.019
Oceania	Australia	75	9.8	1.009	0.060	0.034

Supplementary Table 9 | Maximum acetic acid production cost saving at the corresponding capacity and the production cost at that capacity for 10 countries in fall. For Australia and Chile, hourly weekday electricity prices from March to May 2024 were used, while for other countries, hourly weekday electricity prices from September to November 2023 were used. The average electricity price and its standard deviation for this period are shown for each country.

Fall (March – May 2024 for Australia and Chile | September – November 2023 for other countries)						
		Capacity (%)	Acetic acid production cost saving (%)	Corresponding acetic acid production cost (USD kg^{-1})	Average electricity price (USD kWh^{-1})	Standard deviation of electricity price (USD kWh^{-1})
North America	United States	75	7.2	0.838	0.042	0.020
South America	Chile	37.5	14.8	1.047	0.069	0.032
Europe	Norway	100	0.0	0.944	0.045	0.009
	Denmark	75	5.3	1.355	0.086	0.023
	Spain	62.5	2.9	1.493	0.095	0.018
	France	62.5	5.7	1.521	0.102	0.025
	Germany	62.5	6.7	1.574	0.108	0.028
	Hungary	50	8.6	1.672	0.120	0.034
Asia	Japan	75	4.1	1.419	0.091	0.021
Oceania	Australia	62.5	12.6	1.129	0.075	0.036

Supplementary Table 10 | Maximum acetic acid production cost saving at the corresponding capacity and the production cost at that capacity for 10 countries in winter. For Australia and Chile, hourly weekday electricity prices from June to August 2024 were used, while for other countries, hourly weekday electricity prices from December 2023 to February 2024 were used. The average electricity price and its standard deviation for this period are shown for each country.

Winter (June – August 2024 for Australia and Chile | December 2023 – February 2024 for other countries)						
		Capacity (%)	Acetic acid production cost saving (%)	Corresponding acetic acid production cost (USD kg^{-1})	Average electricity price (USD kWh^{-1})	Standard deviation of electricity price (USD kWh^{-1})
North America	United States	87.5	0.1	0.846	0.037	0.008
South America	Chile	50	9.5	0.885	0.048	0.026
Europe	Norway	87.5	0.2	1.270	0.073	0.012
	Denmark	75	2.1	1.309	0.078	0.017
	Spain	75	2.2	1.226	0.071	0.015
	France	75	1.7	1.300	0.077	0.016
	Germany	75	1.8	1.319	0.079	0.016
	Hungary	62.5	3.5	1.427	0.090	0.020
Asia	Japan	87.5	0.6	1.294	0.075	0.012
Oceania	Australia	50	20.3	1.330	0.106	0.059

Specific Comment R3-2: *To point 2: I expect a full explanation of the TEA method, including every little detail and every assumption on technical and economic inputs. Referring to a published paper simply won't do. Critically, it isn't clear what is included in the capex, does it include equipment costs, or installed costs, or full total capital requirement (ref the DOE/NETL cost estimation guidelines, QGESS). The reason for asking is if not all capital items were included, the capex may easily be double if not triple of what you have calculated, which may alter your analysis and optimal capacity factors quite dramatically. Idem, how was the capex discounted, was a CRF used, or were full NPV calculations done? What is a nominal interest rate? Is it the weighted average cost of capital meant? If so, please use a more realistic value between 7 and 12% (3.7% is a value a government may use, but certainly not a commercial company meaning to make a profit).*

Response: We appreciate the reviewer's suggestion. A full explanation of the TEA method is now included in the Supplementary Information (Supplementary Table 13, Supplementary Notes 3-4). Specifically, the CapEx includes the electrolyzer stack, balance of plant, distillation for liquid product separation, and pressure swing adsorption for gas product separation. The installation factor of 1.12 was applied to the electrolyzer stack. Working capital was assumed to be 5% of the capital cost, and a MACRS 10-year deprecation schedule was used with a 20% salvage value at the end of the plant life. The nominal interest rate was changed from 3.7% to 7% following the reviewer's suggestion.

Page S66:

Supplementary Table 13 | Techno-economic analysis assumptions and parameters for Capital Expenditure (CapEx) and Operating Expenses (OpEx). Detailed calculations for the electrolyzer installed cost and MEA replacement cost can be found in Shin et al.[60], while acetate protonation and electrolyte recovery cost calculations are detailed in Overa et al.[61]

Assumptions	Product production (at 100% capacity)	50,000 kg day^{-1} (Ref[60])
	Factory lifetime	20-year[60]
	Operating time	350 days $year^{-1}$(Ref[60])
	Income tax	0.389[60]
	Nominal interest rate	0.07
	Working capital	5% of total CapEx[60]
	Single pass conversion for acetic acid	50%[62]
CapEx	Base electrolyzer cost	460 USD kW^{-1} (Ref[63])
	E4tech electrolyzer voltage	1.75 V[64]
	E4tech electrolyzer current density	400 mA cm^{-2} (Ref[64])
	Pressure swing adsorption (PSA) reference cost	1,979,043 USD[65]
	PSA reference capacity	1000 m^3 hr^{-1} (Ref[65])
	PSA capacity scaling factor	0.7[65]
	Distillation reference cost – Acetic acid (0.5 M)	9,110,300 USD[61]
	Distillation reference cost – Acetic acid (3 M)	4,421,380 USD[61]
	Distillation capacity scaling factor	0.7[60]
	Balance of Plant	39% of total cost[60]
OpEx	CO cost	0.24 USD kg^{-1}(Ref[62])
	Water cost for OER	0.0054 USD gal^{-1}(Ref[60])
	Maintenance cost	2.5% of electrolyzer CapEx per year[60]
	Cell compartment replacement cost (every 7 year)	15% of electrolyzer CapEx per year[60]
	Cu cost	5.7E-3 USD g^{-1} (Ref[66])
	Cu loading	1 mg cm^{-2} (Ref[62])
	Ni cost	1.2E-2 USD g^{-1} (Ref[67])
	Ni loading	1 mg cm^{-2} (Ref[62])
	Fe cost	7E-5 USD g^{-1} (Ref[68])
	Fe loading	2 mg cm^{-2} (Ref[62])
	Membrane cost	5% of DOE H2A stack cost, 180 USD m^{-2} (Ref[60])
	MEA replacement interval	1 year[60]
	PSA operating cost	0.25 kWh m^{-3} (Ref[65])
	Distillation utility cost – Acetic acid (0.5 M)	17,267,900 USD $year^{-1}$ (Ref[61])
	Distillation utility cost – Acetic acid (3 M)	2,484,690 USD $year^{-1}$ (Ref[61])
	Electricity usage for acetate protonation and KOH regeneration	1.58 kWh kg^{-1} KOH[61]
	KOH : Liquid product acetate	2 :1 molar ratio[61]

Page S70-79:

Supplementary Note 3 | Detailed calculations for techno-economic analysis.

The TEA model in this work is based on previously published models.[60-62,65,70,71] The spreadsheet used to compute production costs, provided in the Supplementary Information of Shin et al.[60] was modified for this work.

a. Capital expenditure (CapEx)

Capital expenditure (CapEx) includes the electrolyzer stack, balance of plant, distillation for liquid product separation, and pressure swing adsorption (PSA) for gas product separation. The sum of these four components is the total depreciable capital. The modified accelerated cost recovery system (MACRS, 10-year schedule) was applied, while the plant lifetime was assumed to be 20 years.[60,65]

For the dynamic operation case, the CapEx and electrolyzer area were set to be the same as those of continuous operation (100% capacity), corresponding to a production rate of 50,000 kg day^{-1}.

1. The electrolyzer stack capital cost:

The electrolyzer stack capital cost assessment followed the methods reported by Shin et al.[60], where the stack cost is obtained by multiplying the reference electrode cost per area by the electrolyzer area:

$$Electrolyzer\ stack\ CapEx\ (USD) = Reference\ electrode\ cost\ per\ area\ \left(\frac{USD}{m^2}\right) \times electrolyzer\ area\ (m^2) \quad (1)$$

The reference electrode cost per area was calculated by adjusting the stack cost from the DOE Current Central H2A model (460 USD kW^{-1})[63]. According to the cost breakdown reported in the E4tech report[72], the cathode and anode originally comprise 25% each of the total stack cost. Thus, we accounted for 50% of the stack cost and added the cathode and anode catalyst costs using the reference electrode area (3125 cm^2). The reference electrolyzer operates at 1.75 V and 0.4 A cm^{-2} (2.19 kW), and the installation factor is 1.12[64]. For this work, the cathode consisted of Cu (5.73E-6 USD mg^{-1})[66] with a loading of 1 mg cm^{-2},[62] and the anode consisted of Ni (1.21E-5 USD mg^{-1})[67] with a loading of 2 mg cm^{-2} [62] and Fe (7.00E-8 USD mg^{-1})[68] with a loading of 1 mg cm^{-2} [62].

Reference cathode cost:

$$Reference\ cathode\ cost = 5.73 \times 10^{-6}\ \left(\frac{USD}{mg}\right) \times 1\ \left(\frac{mg}{cm^2}\right) \times 3125\ cm^2 = 0.018\ USD \quad (2)$$

Reference anode cost:

$$Reference\ anode\ cost = \left(1.21 \times 10^{-5}\ \left(\frac{USD}{mg}\right) \times 2\ \left(\frac{mg}{cm^2}\right) + 7.0 \times 10^{-8} \left(\frac{USD}{mg}\right) \times 1 \left(\frac{mg}{cm^2}\right)\right) \times 3125\ cm^2 = 0.076\ USD \quad (3)$$

Reference electrolyzer cost:

$$Referecne\ electrolyzer\ cost\ \left(\frac{USD}{kW}\right) = \left(460\ \left(\frac{USD}{kW}\right) \times 0.5\right) + \frac{0.018\ USD}{2.19\ kW} + \frac{0.076\ USD}{2.19\ kW} \approx 230\ \left(\frac{USD}{kW}\right) \quad (4)$$

Reference electrode cost per area:

$$Reference\ electrolyzer\ ost\ per\ area\ \left(\frac{USD}{m^2}\right) = 230\left(\frac{USD}{kW}\right) \times \frac{0.4\ A}{cm^2} \times 1.75\ V \times \frac{10^4 cm^2}{m^2} \times \frac{kW}{1000\ W} \times 1.12 \approx 1803\ \left(\frac{USD}{m^2}\right) \quad (5)$$

Electrolyzer area (m^2):

$$Electrolyzer\ area\ (m^2) = Total\ current\ needed\ (A) \times \frac{1}{Current\ density}\left(\frac{1}{\frac{A}{cm^2}}\right) \times \frac{1}{10^4}\left(\frac{m^2}{cm^2}\right) \quad (6)$$

where:

$$Total\ current\ needed\ (A) = Acetic\ acid\ production\ rate\ \left(\frac{kg}{day}\right) \times \frac{day}{24h} \times \frac{1}{Molecular\ weight\ \left(\frac{g}{mol}\right)} \times 4e^- \times F \times \frac{1}{\frac{selectivity}{100}} \quad (7)$$

where $F = 96{,}485\ C\ mol^{-1}$.

2. Balance of plant cost:

Balance of plant cost is assumed to be 39% of the total system cost, with the electrolyzer stack representing 61%[60]:

$$Balance\ of\ Plant = Electrolyzer\ cost \times \frac{0.39}{0.61} \quad (8)$$

3. Distillation capital cost:

$$Distillation\ CapEx\ (USD) = Distillation\ reference\ cost\ (USD) \times \left(\frac{electrolyte\ flow\ rate\ \left(\frac{L}{min}\right)}{Distillation\ reference\ capacity\ \left(\frac{L}{min}\right)}\right)^{0.7} \quad (9)$$

The distillation reference costs are $4,421,380 for a 3 M solution and $9,110,300 for a 0.5 M solution, and the reference capacity is 1000 L min^{-1}.[61]

Electrolyte flow rate:

$$Electrolyte\ flow\ rate\ \left(\frac{L}{min}\right) = Liquid\ product\ flow\ rate\ \left(\frac{L}{min}\right) \div 0.171 \quad (10)$$

Here, 0.171 represents the volume percentage corresponding to 3 M acetic acid. For the 0.5 M acetic acid case, the volume percentage was adjusted accordingly.

$$3\left(\frac{mol}{L}\right) \times 60.052\ \left(\frac{g}{mol}\right) \div 1052\left(\frac{kg}{m^3}\right) \times 1000\ \left(\frac{L}{m^3}\right) \times \frac{1}{1000}\left(\frac{kg}{g}\right) \quad (11)$$

Liquid product flow rate (L min^{-1}):

$$Liquid\ product\ flow\ rate\ \left(\frac{L}{min}\right) = Acetic\ acid\ production\ rate\ \left(\frac{kg}{day}\right) \times \frac{1}{density\left(\frac{kg}{m^3}\right)} \times \frac{1}{24}\left(\frac{day}{h}\right) \times 1000\left(\frac{L}{m^3}\right) \times 60\left(\frac{min}{h}\right) \quad (12)$$

4. PSA capital cost:

$$PSA\ CapEx\ (USD) = PSA\ reference\ cost\ (USD) \times \left(\frac{total\ flow\ rate\ \left(\frac{m^3}{h}\right)}{PSA\ reference\ capacity\ \left(\frac{m^3}{h}\right)}\right)^{0.7} \quad (13)$$

Here, the PSA reference cost is $1,989,043, the reference capacity is 1000 $m^3\ h^{-1}$, and 0.7 is the PSA capacity scaling factor.[65]

Total gas flow rate:

$$Total\ gas\ flow\ \left(\frac{m^3}{h}\right) = CO\ outlet\ flow\ rate\ \left(\frac{m^3}{h}\right) + H_2\ flow\ rate\ \left(\frac{m^3}{h}\right) \quad (14)$$

CO inlet flow rate:

$$CO\ inlet\ flow\ rate\ \left(\frac{kg}{day}\right) = CO\ needed\ \left(\frac{kg}{day}\right) \times \frac{1}{\left(\frac{Conversion}{100}\right)} \quad (15)$$

CO needed:

$$CO\ needed\ \left(\frac{kg}{day}\right) = Acetic\ acid\ production\ rate\ \left(\frac{kg}{day}\right) \times 2 \times \left(\frac{MW_{CO}}{MW_{acetic\ acid}}\right) \quad (16)$$

The conversion was assumed to be 50%.[62]

CO outlet flow rate:

$$CO\ outlet\ flow\ rate\left(\frac{m^3}{h}\right) = CO\ inlet\ flow\ rate\left(\frac{kg}{day}\right)\times \left(1-\frac{Conversion}{100}\right)\times\frac{1}{1.14\left(\frac{kg}{m^3}\right)}\times\frac{1}{24}\left(\frac{day}{h}\right) \quad (17)$$

Hydrogen flow rate:

$$H_2\ flow\ rate\left(\frac{m^3}{h}\right) = Total\ current\ (A)\times\left(1-\frac{Selectivity}{100}\right)\times \frac{1}{2e^-}\times\frac{1}{F}\times 2.008\frac{g}{mol}\times\frac{1}{0.08988\left(\frac{kg}{m^3}\right)}\times\frac{1}{1000}\left(\frac{kg}{g}\right)\times 3600\left(\frac{s}{h}\right) \quad (18)$$

b. Operating expenses (OpEx)

Operating expenses (OpEx) include the electricity cost for electrolyzer operation, electricity cost for power-down, maintenance cost, cell compartment replacement cost, membrane electrode assembly (MEA) replacement cost, CO cost, water usage cost, distillation operation cost, PSA operating cost, and acetate protonation and electrolyte regeneration cost.

3. Electricity cost for electrolyzer operation (100% capacity):

$$Electricity\ cost\ for\ electrolyzer\ operation\left(\frac{USD}{day}\right) = Power\ needed\ (MW)\times\frac{24h}{day}\times electricity\ price\left(\frac{USD}{kWh}\right) \quad (19)$$

where:

$$Power\ needed = Cell\ voltage\ \times\ Total\ current\ needed \quad (20)$$

Where total current needed is calculated using equation (7).

The cell voltage was 2.35 V, and the acetate selectivity was 50%, following the durability test result (Fig. 4a). For dynamic operation, the acetic acid production rate was adjusted according to the operating capacity, resulting in corresponding changes to the total current. The electricity price was also adjusted based on the operating capacity.

4. Electricity cost for power-down:

$$Electricity\ cost_{power\ down}\left(\frac{USD}{day}\right) = Power\ needed_{power\ down}\ (MW)\times Time_{power\ down}\frac{h}{day}\times Electricity\ price_{power\ down}\left(\frac{USD}{kWh}\right) \quad (21)$$

The electricity price used for power-down was the average electricity price during the power-down period, excluding the electricity price during power-on. The current density and voltage during power-down were 10 mA cm^{-2} and 1.9 V,

respectively, based on our power-down experiments (Supplementary Fig. 35a). The electrolyzer area determined from the continuous operation at 50,000 kg day^{-1} (equation (6)) was used to calculate the power needed during power-down.

Power-down time was calculated as:

$$Time_{power\ down} = 24h - Time_{power\ on} \quad (22)$$

For example, at 75% capacity, the power-on time is 18 h and the power-down time is 6 h.

5. Maintenance cost (350 days/year operation):

Maintenance cost was assumed to be 2.5% of the electrolyzer capital cost, with 350 operating days per year.[60]

$$Maintenance\ cost\ \left(\frac{USD}{day}\right) = Electrolyzer\ CapEx\ (USD) \times\ 0.025\ \div \frac{1\ year}{350\ days} \quad (23)$$

6. Cell compartment replacement cost (every 7 years)

Cell compartment replacement cost was assumed to be 15% of the electrolyzer capital cost and to occur every 7 years.[60]

$$Cell\ compartment\ replacement\ cost\ \left(\frac{USD}{day}\right) = Electrolyzer\ CapEx\ (USD) \times\ 0.15\ \div \frac{1\ year}{365\ days} \times \frac{1}{7\ yr} \quad (24)$$

7. Membrane electrode assembly (MEA) replacement cost:

MEA replacement was assumed to occur annually[60].

$$MEA\ replacement\ cost\ \left(\frac{USD}{day}\right) = MEA\ cost\ \left(\frac{USD}{m^2}\right) \times Electrolyzer\ area\ (m^2) \div \frac{1\ year}{365\ days} \quad (25)$$

Where MEA cost (USD m^{-2}) is:

$$\begin{aligned} MEA\ cost\ \left(\frac{USD}{m^2}\right) = \\ Membrane\ cost\ \left(\frac{USD}{m^2}\right) + Cathode\ cost\ \left(\frac{USD}{m^2}\right) + Anode\ cost\ \left(\frac{USD}{m^2}\right) = \\ 180\ \left(\frac{USD}{m^2}\right) + 5.73 \times 10^{-6}\left(\frac{USD}{mg}\right) \times 1\left(\frac{mg}{cm^2}\right) \times 10^4\left(\frac{cm^2}{m^2}\right) \\ + \left(1.21 \times 10^{-5}\left(\frac{USD}{mg}\right) \times 2\left(\frac{mg}{cm^2}\right) + 7.0 \times 10^{-8}\left(\frac{USD}{mg}\right) \times 1\left(\frac{mg}{cm^2}\right)\right) \times 10^4\left(\frac{cm^2}{m^2}\right) \\ = 180.3\ \left(\frac{USD}{m^2}\right) \end{aligned} \quad (26)$$

The electrolyzer area was calculated using equation (6).

8. CO cost:

$$CO\ cost\ \left(\frac{USD}{day}\right) = CO\ needed\ \left(\frac{kg}{day}\right) \times\ CO\ price\ \left(\frac{USD}{ton}\right) \times \frac{1\ ton}{1000\ kg} \quad (27)$$

CO needed is calculated using equation (16). The CO cost was estimated assuming CO generation from an SOEC at 241.4 USD ton^{-1}.[62]

9. Water usage cost:

Water usage was determined from the water consumption required for the oxygen evolution reaction at the anode[60].

$$Water\ usage\ cost\ \left(\frac{USD}{day}\right) = Process\ water\ flow\ \left(\frac{gal}{day}\right) \times\ Process\ water\ cost\ \left(\frac{USD}{gal}\right) \quad (28)$$

where:

$$Process\ water\ flow\ \left(\frac{gal}{day}\right) = Total\ current\ (A) \times \frac{1}{2e^-} \times \frac{1}{F} \times 0.018\left(\frac{kg}{mol}\right) \times 0.2642\left(\frac{gal}{kg}\right) \times 86400\left(\frac{s}{day}\right) \quad (29)$$

10. Distillation operation cost:

$$Distillation\ OpEx\ \left(\frac{USD}{day}\right) = Electrolyte\ flow\ rate\ \left(\frac{L}{min}\right) \div Distillation\ reference\ capacity\ \left(\frac{L}{min}\right) \times Distillation\ OpEx_{reference\ capacity}\ \left(\frac{USD}{day}\right) \quad (30)$$

The electrolyte flow rate was calculated using equation (10). The reference distillation capacity is 1000 L min^{-1} [ref]. The distillation utility costs are 2,484,690 USD year^{-1} for 3 M acetate and 1,267,900 USD year^{-1} for 0.5 M acetate, and the operating time is 350 days year^{-1}.[61]

Operating cost for reference capacity:

$$Distillation\ operating\ cost\ for\ reference\ capacity\ \left(\frac{USD}{day}\right) = Distillation\ utility\ cost\ \left(\frac{USD}{year}\right) \times \frac{1\ year}{350\ day} \quad (31)$$

11. PSA operating cost:

$$PSA\ operating\ cost\ \left(\frac{USD}{day}\right) = Total\ gas\ flow\ \left(\frac{m^3}{h}\right) \times PSA\ operating\ energy\ requirement\ \left(\frac{kWh}{m^3}\right) \times Electricity\ price\ \left(\frac{USD}{kWh}\right) \times 24\ h \quad (32)$$

Total gas flow is calculated from equations (14) – (18). The PSA operating energy requirement is 0.25 kWh m^{-3}.[65]

12. Acetate protonation and electrolyte regeneration cost:

For the KOH electrolyte, the acetate:KOH molar ratio was assumed to be 1:2. [ref] Electricity usage for acetate protonation and electrolyte regeneration followed the methodology of Overa et al.,[61] assuming 1.58 kWh kg^{-1} KOH.

$$Acetate\ protonation\ and\ electrolyte\ regeneration\ cost\ \left(\frac{kWh}{kg_{acetate}}\right) = 1.58\left(\frac{kWh}{kg_{KOH}}\right) \times KOH\ MW\left(\frac{kg_{KOH}}{kmol_{KOH}}\right) \times \left(\frac{2kmol_{KOH}}{1kmol_{acetate}}\right) \div Acetate\ MW\ \approx 3\frac{kWh}{kg_{acetate}} \quad (33)$$

$$Acetate\ protonation\ and\ electrolyte\ regeneration\ cost\ \left(\frac{USD}{day}\right) = 3\left(\frac{kWh}{kg}\right) \times Electricity\ price\ \left(\frac{USD}{kWh}\right) \times acetic\ acid\ production\ rate\ \left(\frac{kg}{day}\right) \quad (34)$$

c. Discounted cash flow analysis

The discounted cash flow analysis was applied with an income tax rate of 0.389[65], and a nominal interest rate of 0.07. It was assumed that construction of the facility is completed in the first year, with product production beginning in the second year. Working capital was assumed to be 5% of the capital cost, and a MACRS 10-year depreciation schedule was used with a 20% salvage value at the end of the plant life.[65] Finally, the production cost was determined by evaluating a selling price that resulted in a net present value of zero at the end of the process life.

Supplementary Note 4 | Choices of 10 countries globally for techno-economic analysis.

Ten countries were selected globally based on the availability of hourly electricity price data on the IEA website. For North America, the United States was selected from the two available countries (the United States and Mexico). For South America, Chile was selected due to its distinct binary-shaped hourly electricity price profile (Supplementary Fig. 45 a, c, e, g). Europe has the largest number of available countries on the IEA website. Norway was chosen because 89% of its electricity generation comes from non-intermittent renewable sources (hydropower) (Supplementary Fig. 42[11]), while Denmark was selected as another Northern European country where 92% of electricity generation is from renewables, with variable renewable energy accounting for 69%[73]. Spain, France, Germany, and Hungary were also selected as European countries for the analysis. For Asia, Japan was selected from the two available countries (Japan and Philippines). For Oceania, Australia was the only available country on the IEA website.

Point-by-Point Response to Review Comments

Reviewer: 1

General Comments R1: *The authors have done a fantastic job in addressing the reviewers questions. The work is ready for publication.*

Response: We thank the reviewer for the positive and encouraging comments. We are pleased that the reviewer finds the work suitable for publication.

Reviewer: 2

General Comments R2: *I have carefully reviewed the authors' responses and the revised manuscript. The authors have addressed all of my concerns and questions in a satisfactory manner. The revisions have significantly improved the clarity and quality of the work. I have no further comments and recommend the paper for publication. Figure 2 is currently not very aesthetically pleasing and could be better formatted.*

Response: We thank the reviewer for the careful and positive assessment of our revised manuscript and for recommending it for publication. We are pleased that all concerns have been satisfactorily addressed. In response to the comment on Figure 2, we have revised the layout and formatting to improve its visual clarity and overall presentation.

Reviewer: 3

General Comments R3: *The reviewer appreciates the changes made to the TEA section, but it remains unclear if all relevant costs are included in the model. The question to what extent cyclic operation is economical is a critical one, and deserves careful consideration. Only if all relevant capital and operational costs are included, the analysis is meaningful. In the current rebuttal and revised manuscript, it remains unclear if they are. Authors suggest they include costs for the electrolyser, balance of plant, distillation and PSA. This is not disputed. What is unclear is if ALL costs are included for these unit operations. Referring to the DOE/NETL studies and guidelines (QGESS, I referred to this in my previous reply but the authors failed to comments on this), a full capital cost should amount at Total Capital Required, also called Total As Spent Cost. This includes equipment, installation, EPC, appropriate contingencies (not the obligatory 10% everybody adds), owner's and start up costs, and interest during construction. Only if all these capital elements are included, can a meaningful analysis of part-load operation be undertaken. From the current reply, and digging into the SI references cites (60-63 mainly), here, only the equipment and installation costs are included. If true, the real capital required would be 2-3 times higher, rendering a completely different part-load analysis.*

Failing to comment on this suggests authors may be unaware of this point, which leads the reviewer to dismiss the manuscript as suitable for publication (and I even wonder if all previous Nature Catalysis and Sustainability publications using the same TEA model should not be retracted too).

I'm afraid I have to recommend against publication.

Response: We agree that incorporating the full capital cost build-up in accordance with DOE/NETL QGESS guidance will further strengthen the techno-economic assessment of the dynamic operation process. In the revised manuscript and Supplementary Information, we have now explicitly incorporated all relevant capital components to calculate the Total As-Spent Cost (TASC), including:

- Equipment costs
- Installation factors for each unit operation
- Bare Erected Cost (BEC)
- Engineering, Procurement, and Construction Cost (EPCC)
- Process contingency
- Project contingency
- Total Plant Cost (TPC)

- Owner's costs
- Interest During Construction (IDC)
- Total Overnight Cost (TOC)
- Total As-Spent Cost (TASC)

The complete capital build-up methodology is now detailed in Supplementary Note 3, with parameters summarized in Supplementary Table 13 and sensitivity ranges provided in Supplementary Table 14.

After incorporating all capital elements following NETL QGESS guidance, the updated total capital requirement is higher than the initial estimate reported in the previous revision. We thank the reviewer for this comment, which allowed us to improve the accuracy of the TEA model.

Under the fully built-up capital structure and across conservative sensitivity scenarios, dynamic operation still provides substantial economic benefits in regions with high electricity price variability (e.g., South Australia). A sensitivity analysis of CapEx assumptions has been performed (Supplementary Fig. 42), demonstrating that dynamic operation remains economically advantageous under both optimistic and most pessimistic capital scenarios.

The revised manuscript and Supplementary Information now clearly present:

1. The complete capital cost derivation through TASC
2. Explicit alignment with NETL QGESS methodology
3. Sensitivity analysis over installation factors, EPCM, and contingencies
4. Inclusion of operation labor costs within OpEx
5. Updated production cost results using the revised CapEx

We hope this revision fully addresses the reviewer's concern regarding capital completeness and strengthens the robustness and transparency of the economic conclusions. All the modification could be found in the manuscript Page 11, 12, S67-69, and S73-78.

Page 11:

Varying the operational capacity and corresponding electricity prices, as well as the standard deviation of electricity prices, significantly affect acetic acid production costs (Fig. 5). We compared the cases of South Australia and Norway, representing intermittent renewable energy with high electricity price variability and non-intermittent renewable energy with low variability, respectively (Fig. 5a). For South Australia, where intermittent renewable energy sources are utilized, operating at 62.5% capacity yielded the lowest production cost at 1.63 USD kg^{-1}, representing a 26% cost saving relative to the full capacity cost of 2.13 USD kg^{-1} by avoiding peak electricity prices (Fig. 5a, Supplementary Fig. 41a). Even operation at 37.5% capacity resulted in a 16% cost saving (1.83 USD kg^{-1}) compared to full capacity, due to the high contribution of electricity costs for the electrolyzer at full capacity, which accounted for more than 52% of the overall cost (Supplementary Fig. 41a). Operating at 62.5% capacity enabled production cost savings by utilizing low-cost electricity while reducing the capital expense contribution to 22% of the overall cost (Supplementary Fig. 41a). The electricity used during the power-down period remained less than 1% of production cost for various operating capacities (Supplementary Fig. 41a). Capital expenditure (CapEx) plays a key role in determining whether dynamic operation is economically viable, as CapEx is not fully utilized when the capacity factor is reduced. To address uncertainties in the CapEx estimation, a sensitivity analysis was performed for the South Australia case. From the optimistic to the most pessimistic scenario, dynamic operation still resulted in acetic acid production cost savings (optimistic case: a 62.5% capacity factor yielded 27% savings; most pessimistic case: a 75% capacity factor yielded 19% savings relative to operation at 100% capacity) (Supplementary Fig. 42, Supplementary Table 14, Supplementary Note 3). For the remaining analyses, the base case CapEx was applied.

Page 12:

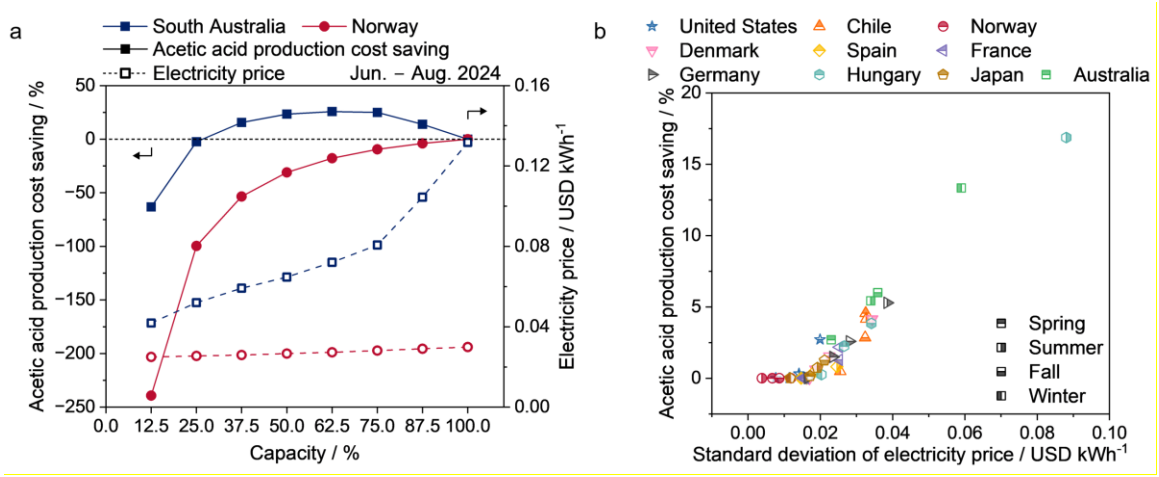

Fig. 5 | Techno-economic analysis of dynamic and steady state operation of CO electrolyzers for acetic acid production. a | Comparison of South Australia (intermittent renewables, high standard deviation in electricity price: 0.097 USD kWh^{-1}) and Norway (non-intermittent renewables, low standard deviation in electricity price: 0.004 USD kWh^{-1}). The left y-axis shows the acetic acid production cost saving relative to 100% capacity (with 100% capacity corresponding to 50,000 kg day^{-1}), while the right y-axis displays the corresponding weekday electricity price in South Australia[44] and Norway from June to August 2024[46]. **b** | Acetic acid production cost saving as a function of the standard deviation of electricity price for 10 countries worldwide, evaluated across four seasons (spring, summer, fall, and winter) from September 2023 to August 2024. The base case CapEx (Supplementary Table 14, Supplementary Note 3) was assumed in this analysis.

Supplementary Information. Page 43:

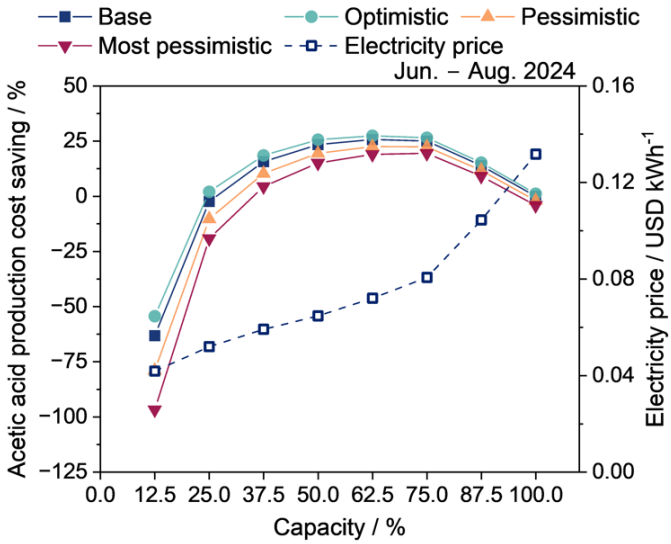

Supplementary Fig. 42 | Sensitivity analysis of capital expenditure (CapEx) for the South Australia case. The corresponding sensitivity parameters are listed in Supplementary Table 14.

Supplementary Information. Page 67-69:

Supplementary Table 13 | Techno-economic analysis assumptions and parameters for Capital Expenditure (CapEx) and Operating Expenses (OpEx). Detailed calculations for the electrolyzer installed cost and MEA replacement cost can be found in Shin et al.[60], while acetate protonation and electrolyte recovery cost calculations are detailed in Overa et al.[61]

Assumptions	Product production (at 100% capacity)	50,000 kg day^{-1} (Ref[60])
	Factory lifetime	20-year[60]
	Operating time	350 days $year^{-1}$(Ref[60])
	Income tax	0.389[60]
	Nominal interest rate	0.07
	Working capital	5% of TOC[60]
	Single pass conversion for acetic acid	50%[62]
CapEx – Bare Erected Cost (BEC): base case	Base electrolyzer cost	460 USD kW^{-1} (Ref[63])
	E4tech electrolyzer voltage	1.75 V[64]
	E4tech electrolyzer current density	400 mA cm^{-2} (Ref[64])
	Electrolyzer installation factor	1.12[64]
	Pressure swing adsorption (PSA) reference cost	1,979,043 USD[65]
	PSA reference capacity	1000 m^3 hr^{-1} (Ref[65])
	PSA capacity scaling factor	0.7[65]
	PSA installation factor	1
	Distillation reference cost – Acetic acid (0.5 M)	9,110,300 USD[61]
	Distillation reference cost – Acetic acid (3 M)	4,421,380 USD[61]
	Distillation capacity scaling factor	0.7[60]
	Distillation installation factor	1
	Balance of Plant	39% of total electrolyzer system cost[60]
CapEx – Engineering, Procurement and Construction Cost (EPCC): base case	Engineering, procurement and construction management (EPCM) contractor service	18% of BEC[66]
CapEx – Total Plant Cost (TPC): base case	Process contingency	25% of BEC[66]
	Project contingency	20% of the sum of BEC, EPC fees, and process contingency[66]
CapEx – Total Overnight Cost (TOC): base case	Owner's cost	20% of TPC[66]
CapEx – Total As-Spent Cost (TASC): base case	Interest during construction (IDC)	~3.44%

OpEx	CO cost	0.24 USD kg^{-1}(Ref[62])
	Water cost for OER	0.0054 USD gal^{-1}(Ref[60])
	Maintenance cost	2.5% of electrolyzer CapEx per year[60]
	Cell compartment replacement cost (every 7 year)	15% of electrolyzer CapEx per year[60]
	Cu cost	5.7E-3 USD g^{-1} (Ref[67])
	Cu loading	1 mg cm^{-2} (Ref[62])
	Ni cost	1.2E-2 USD g^{-1} (Ref[68])
	Ni loading	1 mg cm^{-2} (Ref[62])
	Fe cost	7E-5 USD g^{-1} (Ref[69])
	Fe loading	2 mg cm^{-2} (Ref[62])
	Membrane cost	5% of DOE H2A stack cost, 180 USD m^{-2} (Ref[60])
	MEA replacement interval	1 year[60]
	PSA operating cost	0.25 kWh m^{-3} (Ref[65])
	Distillation utility cost – Acetic acid (0.5 M)	17,267,900 USD $year^{-1}$ (Ref[61])
	Distillation utility cost – Acetic acid (3 M)	2,484,690 USD $year^{-1}$ (Ref[61])
	Electricity usage for acetate protonation and KOH regeneration	1.58 kWh kg^{-1} KOH[61]
	KOH : Liquid product acetate	2 :1 molar ratio[61]
	Operating labor – base labor rate	38.5 USD h^{-1} (Ref[70])
	Operating labor – Associated labor burden	30% of the base labor rate[70]
	Operating labor – Administration and overhead	25% of the burdened labor rate[70]
	Operating labor – Operators per day	5[70]

Supplementary Table 14 | Capital Expenditure (CapEx) parameters used for sensitivity analysis of the South Australia case (Supplementary Fig. 42). Additional details on the CapEx calculation are provided in Supplementary Note 3.

	Base case	Optimistic case	Pessimistic case	Most pessimistic case
Installation factor for PSA (f_{PSA})	1	1	1	1.17[71]
Installation factor for distillation ($f_{distillation}$)	1	1	1	2.47[72]
EPCM contractor service (f_{EPCM})[66]	18%	15%	20%	20%
EPCC[66]	1.18 BEC	1.15 BEC	1.20 BEC	1.20 BEC
[66]	25%	20%	35%	35%
Process contingency	0.25 BEC	0.20 BEC	0.35 BEC	0.35 BEC
Project contingency factor ($f_{project}$)[66]	20%	15%	30%	30%
Project contingency[66]	0.2 (BEC + 0.18 BEC + 0.25 BEC) = 0.286 BEC	0.15 (BEC + 0.15 BEC + 0.20 BEC) = 0.2025 BEC	0.3 (BEC + 0.2 BEC + 0.35 BEC) = 0.465 BEC	0.3 (BEC + 0.2 BEC + 0.35 BEC) = 0.465 BEC
TPC[66]	1.18 BEC + 0.25 BEC + 0.286 BEC = 1.716 BEC	1.15 BEC + 0.2 BEC + 0.2025 BEC = 1.5525 BEC	1.2 BEC + 0.35 BEC + 0.465 BEC = 2.015 BEC	1.2 BEC + 0.35 BEC + 0.465 BEC = 2.015 BEC
Owner's cost factor (f_{owner})[66]	20%	20%	20%	20%
Owner's cost[66]	0.2 TPC = 0.3432 BEC	0.2 TPC = 0.3105 BEC	0.2 TPC = 0.403 BEC	0.2 TPC = 0.403 BEC
TOC[66]	~2.06 BEC	~1.86 BEC	~2.42 BEC	~2.42 BEC
TASC	1.034 TOC = ~2.13 BEC	1.034 TOC = ~1.93 BEC	1.034 TOC = ~2.50 BEC	1.034 TOC = ~2.50 BEC

Supplementary Information. Page 73 – 78:

Supplementary Note 3 | Detailed calculations for techno-economic analysis.

The TEA model in this work is based on previously published models.[60-62,65,74,75] The spreadsheet used to compute production costs, provided in the Supplementary Information of Shin et al.[60] was modified for this work.

a. Capital expenditure (CapEx)

1. Bare Erected Cost (BEC)

Bare Erected Cost (BEC) includes the electrolyzer stack, balance of plant (BoP), distillation for liquid product separation, and pressure swing adsorption (PSA) for gas product separation. For the dynamic operation case, the electrolyzer area and BEC were assumed to be identical to those of continuous operation (100% capacity), corresponding to a production rate of 50,000 kg day^{-1}. The BEC was estimated as:

$$BEC = Installed\ electrolyer\ stack + Balance\ of\ plant + Installed\ distillation + Installed\ PSA \quad (1)$$

i. The electrolyzer stack BEC:

The electrolyzer stack equipment cost assessment followed the methods reported by Shin et al.[60], where the stack cost is obtained by multiplying the reference electrode cost per area by the electrolyzer area:

$$Electrolyzer\ stack\ equipment\ cost\ (USD) = Reference\ electrode\ cost\ per\ area\ \left(\frac{USD}{m^2}\right) \times electrolyzer\ area\ (m^2) \quad (2)$$

The reference electrode cost per area was calculated by adjusting the stack cost from the DOE Current Central H2A model (460 USD kW^{-1})[63]. According to the cost breakdown reported in the E4tech report[64], the cathode and anode originally comprise 25% each of the total stack cost. Thus, we accounted for 50% of the stack cost and added the cathode and anode catalyst costs using the reference electrode area (3125 cm^2). The reference electrolyzer operates at 1.75 V and 0.4 A cm^{-2} (2.19 kW). To estimate the BEC of the electrolyzer stack, an installation factor of 1.12 was applied to the stack equipment cost[64]. For this work, the cathode consisted of Cu (5.73E-6 USD mg^{-1})[67] with a loading of 1 mg cm^{-2},[62] and the anode consisted of Ni (1.21E-5 USD mg^{-1})[68] with a loading of 2 mg cm^{-2} [62] and Fe (7.00E-8 USD mg^{-1})[69] with a loading of 1 mg cm^{-2} [62].

Reference cathode cost:

$$Reference\ cathode\ cost = 5.73 \times 10^{-6}\ \left(\frac{USD}{mg}\right) \times 1\ \left(\frac{mg}{cm^2}\right) \times 3125\ cm^2 = 0.018\ USD \quad (3)$$

Reference anode cost:

$$Reference\ anode\ cost = \left(1.21 \times 10^{-5}\ \left(\frac{USD}{mg}\right) \times 2\ \left(\frac{mg}{cm^2}\right) + 7.0 \times 10^{-8} \left(\frac{USD}{mg}\right) \times 1 \left(\frac{mg}{cm^2}\right)\right) \times 3125\ cm^2 = 0.076\ USD \quad (4)$$

Reference electrolyzer cost:

$$Referecne\ electrolyzer\ cost\ \left(\frac{USD}{kW}\right) = \left(460\ \left(\frac{USD}{kW}\right) \times 0.5\right) + \frac{0.018\ USD}{2.19\ kW} + \frac{0.076\ USD}{2.19\ kW} \approx 230\ \left(\frac{USD}{kW}\right) \quad (5)$$

Reference electrode cost per area:

$$Reference\ electrolyzer\ ost\ per\ area\ \left(\frac{USD}{m^2}\right) = 230 \left(\frac{USD}{kW}\right) \times \frac{0.4\ A}{cm^2} \times 1.75\ V \times \frac{10^4 cm^2}{m^2} \times \frac{kW}{1000\ W} \times 1.12 \approx 1803\ \left(\frac{USD}{m^2}\right) \quad (6)$$

Electrolyzer area (m^2):

$$Electrolyzer\ area\ (m^2) = Total\ current\ needed\ (A) \times \frac{1}{Current\ density} \left(\frac{1}{\frac{A}{cm^2}}\right) \times \frac{1}{10^4} \left(\frac{m^2}{cm^2}\right) \quad (7)$$

where:

$$Total\ current\ needed\ (A) = Acetic\ acid\ production\ rate\ \left(\frac{kg}{day}\right) \times \frac{day}{24h} \times \frac{1}{Molecular\ weight\ \left(\frac{g}{mol}\right)} \times 4e^{-} \times F \times \frac{1}{\frac{selectivity}{100}} \quad (8)$$

where $F = 96{,}485\ C\ mol^{-1}$.

ii. Balance of plant BEC

Balance of plant cost was assumed to be 39% of the total electrolyzer system cost, with the electrolyzer stack representing the remaining 61%[60]:

$$Balance\ of\ Plant = Installed\ electrolyzer\ cost \times \frac{0.39}{0.61} \quad (9)$$

iii. Distillation BEC:

$$Distillation\ equipment\ cost\ (USD) = Distillation\ reference\ cost\ (USD) \times \left(\frac{electrolyte\ flow\ rate\ \left(\frac{L}{min}\right)}{Distillation\ reference\ capacity\ \left(\frac{L}{min}\right)}\right)^{0.7} \quad (10)$$

The distillation reference costs are $4,421,380 for a 3 M solution and $9,110,300 for a 0.5 M solution, and the reference capacity is 1000 L min^{-1}.[61]

Electrolyte flow rate:

$$Electrolyte\ flow\ rate\ \left(\frac{L}{min}\right) = Liquid\ product\ flow\ rate\ \left(\frac{L}{min}\right) \div 0.171 \quad (11)$$

Here, 0.171 represents the volume percentage corresponding to 3 M acetic acid. For the 0.5 M acetic acid case, the volume percentage was adjusted accordingly.

$$3\left(\frac{mol}{L}\right) \times 60.052\ \left(\frac{g}{mol}\right) \div 1052\left(\frac{kg}{m^3}\right) \times 1000\ \left(\frac{L}{m^3}\right) \times \frac{1}{1000}\left(\frac{kg}{g}\right) \quad (12)$$

Liquid product flow rate (L min^{-1}):

$$Liquid\ product\ flow\ rate\ \left(\frac{L}{min}\right) = Acetic\ acid\ production\ rate\ \left(\frac{kg}{day}\right) \times \frac{1}{density\left(\frac{kg}{m^3}\right)} \times \frac{1}{24}\left(\frac{day}{h}\right) \times 1000\left(\frac{L}{m^3}\right) \times 60\left(\frac{min}{h}\right) \quad (13)$$

Since the distillation CapEx was obtained from the literature[61] and it was unclear whether the reported value corresponded to the bare equipment cost or the installed cost (i.e., BEC in this work), an installation factor of 1.0 was assumed in the base case, treating the literature value as an installed (BEC-level) cost. A sensitivity analysis was conducted to evaluate the case in

which the literature CapEx represented the bare equipment cost, and an installation factor of 2.47[72] was applied accordingly (Supplementary Fig. 42, Supplementary Table 14).

iv. PSA capital cost:

$$PSA\ CapEx\ (USD) = PSA\ reference\ cost\ (USD) \times \left(\frac{total\ flow\ rate\ \left(\frac{m^3}{h}\right)}{PSA\ reference\ capacity\ \left(\frac{m^3}{h}\right)}\right)^{0.7} \quad (14)$$

Here, the PSA reference cost is $1,989,043, the reference capacity is 1000 $m^3\ h^{-1}$, and 0.7 is the PSA capacity scaling factor.[65]

Total gas flow rate:

$$Total\ gas\ flow\ \left(\frac{m^3}{h}\right) = CO\ outlet\ flow\ rate\ \left(\frac{m^3}{h}\right) + H_2\ flow\ rate\ \left(\frac{m^3}{h}\right) \quad (15)$$

CO inlet flow rate:

$$CO\ inlet\ flow\ rate\ \left(\frac{kg}{day}\right) = CO\ needed\ \left(\frac{kg}{day}\right) \times \frac{1}{\left(\frac{Conversion}{100}\right)} \quad (16)$$

CO needed:

$$CO\ needed\ \left(\frac{kg}{day}\right) = Acetic\ acid\ production\ rate\ \left(\frac{kg}{day}\right) \times 2 \times \left(\frac{MW_{CO}}{MW_{acetic\ acid}}\right) \quad (17)$$

The conversion was assumed to be 50%.[62]

CO outlet flow rate:

$$CO\ outlet\ flow\ rate\ \left(\frac{m^3}{h}\right) = CO\ inlet\ flow\ rate\ \left(\frac{kg}{day}\right) \times \left(1 - \frac{Conversion}{100}\right) \times \frac{1}{1.14\left(\frac{kg}{m^3}\right)} \times \frac{1}{24}\left(\frac{day}{h}\right) \quad (18)$$

Hydrogen flow rate:

$$H_2\ flow\ rate\ \left(\frac{m^3}{h}\right) = Total\ current\ (A) \times \left(1 - \frac{Selectivity}{100}\right) \times \frac{1}{2e^-} \times \frac{1}{F} \times 2.008\frac{g}{mol} \times \frac{1}{0.08988\ \left(\frac{kg}{m^3}\right)} \times \frac{1}{1000}\left(\frac{kg}{g}\right) \times 3600\left(\frac{s}{h}\right) \quad (19)$$

Similar to the distillation CapEx, the PSA CapEx was obtained from the literature[65], and the reported cost basis (bare equipment cost vs. installed cost) was not explicitly specified. In the base case, an installation factor of 1.0 was assumed, treating the literature value as an installed (BEC-level) cost. A sensitivity analysis was performed to evaluate the case in which

the literature CapEx represented the bare equipment cost, and an installation factor of 1.17[71] was applied (Supplementary Fig. 42, supplementary Table 14).

2. Engineering, Procurement, and Construction Cost (EPCC)

Engineering, procurement, and construction management (EPCM) contractor services (f_{EPCM}) were assumed to be 18% of the BEC in the base case. A sensitivity analysis was conducted by varying the EPCM contractor service factor from 15% to 20%, consistent with the NETL guidance[66].

$$EPCC = BEC \times (1 + f_{EPCM}) \quad (20)$$

3. Total Plant Cost (TPC).

The total plant cost (TPC) was calculated by incorporating both process and project contingencies. The process contingency factor ($f_{process}$) was assumed to be 25%, reflecting a technology maturity level corresponding to small pilot-scale data[66], as a 10 kW electrolyzer system has been demonstrated[76]. A sensitivity analysis was conducted by varying $f_{process}$ from 20% to 35%.

The project contingency factor ($f_{project}$) was assumed to be 20%. Consistent with AACE/NETL guidance[66], the project contingency was calculated as 20% of the sum of BEC, EPCM cost, and process contingency. A sensitivity analysis was performed by varying $f_{project}$ from 15% to 30%.

The TPC was calculated as:

$$TPC = EPCC + f_{procss} \times BEC + f_{project} \times \left(BEC + f_{EPCM} \times BEC + f_{process} \times BEC\right) \quad (21)$$

4. Total Overnight Cost (TOC)

The owner's cost factor (f_{owner}) was assumed to be 20%[66], and owner's costs were calculated as:

$$Owner^{'}s\ costs = f_{owner} \times TPC \quad (22)$$

The total overnight cost (TOC) was then calculated as:

$$TOC = TPC + Owner^{'}s\ costs \quad (23)$$

5. Total As-Spent Cost (TASC)

The total as-spent cost (TASC) was estimated by accounting for interest during construction (IDC). A one-year construction period was assumed[65], with expenditures occurring on average at mid-year. A nominal interest rate of 7% was applied.

IDC was calculated as:

$$(1.07)^{0.5} - 1 = 0.0344 = 3.44\% \quad (24)$$

The TASC was then calculated as:

$$TASC = TOC + IDC \times TOC \approx 1.034 \times TOC \quad (25)$$

a. Operating expenses (OpEx)

Operating expenses (OpEx) include the electricity cost for electrolyzer operation, electricity cost for power-down, maintenance cost, cell compartment replacement cost, membrane electrode assembly (MEA) replacement cost, CO cost, water usage cost, distillation operation cost, PSA operating cost, acetate protonation and electrolyte regeneration cost, and operation labor cost.

This manuscript proposes and validates that under dynamic electrolysis conditions (mimicking fluctuating renewable electricity), Cu cathodes undergo deactivation due to surface CO oxidation during shutdown, leading to the formation of (bi)carbonate, or through oxidation into Cu_2O at open-circuit potential under an inert atmosphere. To address this issue, the authors introduce a mitigation strategy by maintaining a slightly negative potential relative to OCP (corresponding to ~1.8-1.9 V for the full cell) during shutdown, which effectively suppresses carbonate formation and oxidation. Experimentally, this approach enables stable dynamic operation for more than 300 hours, accompanied by a techno-economic analysis (TEA) that demonstrates its feasibility. The study integrates in-situ Raman, CV, XAS, DFT, and TEA, presenting a comprehensive investigation with practical engineering relevance. Nonetheless, a few important issues remain to be clarified.

1. The main experiments employ commercial Cu powder (40-60 nm), with a small amount of micron-sized Cu as a comparison. However, Cu in practice exhibits diverse surface structures, crystal facets, roughness, and oxide-derived precursors, all of which can significantly influence CO adsorption, OH* adsorption, and the propensity for carbonate formation.
2. During power-down the authors reduce the CO feed to 2 $mL \cdot min^{-1}$ and the anolyte flow to 0.1 $mL \cdot min^{-1}$ while maintaining the full-cell potential at 1.9 V. It is unclear whether this 'reduced-flow + maintained-potential' protocol is practicable at industrial scale or whether the TEA fully accounts for the operational implications of such an approach.
3. The SERS spectra exhibit a peak at 1085 cm^{-1}, which the authors assign to carbonate species. However, no direct evidence of transient CO_2 release during OCP or quantitative monitoring of the chemical species via online analysis is provided. The author should detect whether there is a CO_2 overflow peak in the OCP phase and verify the chemical bonding state and coverage of surface carbonate/carbonate ions or use ATR-FTIR to further confirm the carbonic acid/bicarbonate peak.
4. The long-term stability and durability data (>cs300 h) appear to be derived from a single demonstration, with no information provided on the number of repetitions or the associated error margins. For claims of "industrializable" stability, reproducibility data are indispensable.
5. When the power-down period is extended to 7 days, the performance becomes irreversible, indicating the presence of irreversible damage. Is this irreversible degradation still attributable to carbonate poisoning? If so, why cannot it be recovered in the same manner as short-term shutdown? If not, what are the underlying causes?
6. Applying a protective potential inevitably alters the overall cell state and may exert long-term effects on the NiFeOx anode or the membrane. However, the manuscript does not provide long-term monitoring data on membrane impedance or anode stability.
7. The authors employ a four-layer Cu (100) slab with the PBE-D3 functional and the CHE

method to calculate the pathway, reporting both ΔG and ΔG‡. However, it is well known that the CHE approach and conventional constant-potential DFT carry inherent limitations when modeling charged interfaces, explicit solvent effects, and high OH^- concentrations (pH 14). Potential-dependent adsorption energies, solvation effects, and interfacial charge distributions can significantly affect both adsorption energetics and reaction barriers.

8. The calculations are restricted to the Cu (100) surface, while other facets such as (111), (110), step/edge, and grain-boundary sites are neglected. These sites may exhibit distinct reaction pathways and barriers, as also suggested by experimental evidence indicating facet-dependent responses. Although the authors briefly mention this possibility, no calculations were performed to substantiate it.
9. The manuscript contains careless omissions of units. For example, the sentence "The subsequent electrosorption of CO_3^{2-}(aq) releases an energy of ΔG = -1.13" lacks the unit of ΔG. The authors must carefully check the entire manuscript (main text, figures, tables and Supporting Information) and correct all instances where physical/chemical quantities are missing units.